Effect of Shimming on Fatigue Life

A project presented to
The Faculty of the Department of Aerospace Engineering
San José State University

In partial fulfillment of the requirements for the degree
Master of Science in Aerospace Engineering

by

Anushree Gharat

May 2025

approved by

Prof. Maria Chierichetti
Faculty Advisor

ABSTRACT

The Design of Effect of Shimming on Fatigue Life

Anushree Gharat

This paper reports on a finite element study of the effect of an epoxy resin shim on the characteristics of fatigue performance of aluminum alloy components, using ANSYS Workbench 19.2. The finite element study consisted of two configurations, a monolithic aluminum alloy structure, and a shimmed configuration (which includes an epoxy resin shim) both models were loaded under the same loading and boundary conditions. These two configurations ultimately necessitated two configurations be developed where the mechanical effect of the shim could be isolated.

Mesh convergence studies were undertaken with both configurations to further understand the stability of the solution using stress, strain and deformation analysis to ensure the data is reliable and accurate. The fatigue performance evaluation was performed using the strain-life (ε-N) method with the Morrow mean stress correction. The results from the study indicate that epoxy resin shimming not only reduces areas of high stress concentration, provides evidence for strain distribution across the structure, but most importantly proves that it vastly improves fatigue resistance properties while subjected to cyclic loading.

ACKNOWLEDGEMENT

The author would like to express appreciation to the faculty and staff of the Department of Aerospace Engineering for their assistance and guidance in furthering this Master's project. The author sincerely thanks San Jose State University for providing access to the ANSYS software and computational resources that made this project possible. Special thanks are due to Professor Maria Chierichetti for her invaluable mentorship and technical advice. The authors are also thankful to their graduate colleagues for their useful discussions and suggestions during this work. Finally, the authors would like to thank their families for their support and encouragement.

TABLE OF CONTENTS

LIST OF FIGURE

LIST OF TABLES

NOMENCLATURE

SYMBOL	DEFINITION	UNITS
σ	Stress Tensor	N/m^2 (Pa)
ϵ	Strain Tensor	
ε	Strain	
ρ	Density	kg/m^3
u	Displacement Vector	m
c	Specific Heat	J/kgK
q	Heat Flux	W/m^2
k	Thermal Conductivity	W/mK
F	External Forces	N
E	Modulus of Elasticity	N/m^2
T	Temperature	K
Q	Internal Heat Source	J
σ_a	Stress Amplitude	Pa
σ'_f	Fatigue Strength Coefficient	Pa
N_f	Number of Cycles to Failure	cycle
b	Fatigue Strength Exponent	
σ_m	Mean Stress	Pa
σ_f	Fatigue Strength	Pa
σ_u	Ultimate Tensile Strength	Pa
D	Fatigue Damage	

n_i	Number of Applied Cycles	cycles
N_i	Corresponding Fatigue Life	cycles
ε_a	Strain Amplitude	
ε'_f	Fatigue Ductility Coefficient	
c	Fatigue Ductility Exponent	
da/dN	Crack Growth Rate per Cycle	m/cycle
ΔK	Stress Intensity Factory Range	$Pa.m^{1/2}$
C, m	Paris' Law Constant	
E_n	Percentage Error between Mesh Refinements	%
Q_n	Computed Value (current mesh size)	
Q_{n-1}	Computed Value (previous mesh size)	
σ_{max}	Maximum Stress	Pa
ε_{max}	Maximum Strain	
σ_{min}	Minimum Stress	Pa
ε_{min}	Minimum Strain	
R	Load Ratio	

I. Introduction

Modern aerospace engineering represents a fascinating intersection of advanced materials and sophisticated analytical methods, as exemplified by the Boeing 787 Dreamliner's development and analysis. Hailed as one of the great technological breakthroughs in aerospace engineering, this aircraft was, as the first, manufactured in unthinkable dimensions with composite materials. The crux of the innovation lies in the Carbon Fiber Reinforced Polymers (CFRPs), developed especially to provide high strength-to-weight ratios for better operational performance and fuel economy.

1.1 Literature Review

Aluminum alloys have been a primary material in aerospace engineering because they are low density and high strength, corrosion-resistant and malleable. They have been the material of choice in all of aerospace when performance and weight needed to be minimized, especially airframe structural components. Aviation usage of aluminum can be traced back to the first planes of the 19th century, and the understanding of this material was greatly improved during WW II. The first alloy developed that became widely accepted for aerospace use was duralumin (Al-Cu), before the introduction of higher-performing aluminum alloy series such as the 2000 and 7000 series [1].

The 2000 series aluminum alloys including 2024-T3 represent an aluminum-copper system which has good fatigue strength and fracture toughness. These are well suited to fuselage skins, wing panels and structures and components under cyclic loading. The 7000 series alloys such as 7075-T6 and 7050 7451, are aluminum-zinc-magnesium alloys which have very high tensile strength. They are frequently used in high-stress critical structural applications like wing spars and supporting structures for landing gears. The introduction of advanced processing and heat treatment techniques, each have contributed to their improvements and the reduced potential for loss of structural integrity due to stress-corrosion cracking [2].

The mechanical properties of these alloys can be considerably changed on heat treatment, either through solution heat treatment, age hardening, and annealing. This gives an engineer the ability to customize the yield strength, ductility and fatigue life of components made of aluminum alloy so that they are in line with the desired performance specifications. A common tempering for aluminum alloys such as 6061 and 7075, is T6 (solution heat treated and artificial aging), because it is often a good compromise between strength and toughness [3].

The aerospace industry also began to look into alloying aluminum with lithium and the effects this has in improving the modulus of aluminum while lowering the density. Al-Li alloys like AA2195 and AA2090 have found uses in commercial and space aviation with notable reductions in weight from normal aluminum alloys of approximately 10% with comparable fatigue strength [4].

New fabrication technologies such as friction stir welding (FSW) have also enhanced fatigue properties for structural joints. FSW employs mechanisms that eliminate defects that come with fusion, while keeping the fine grain structure intact, resulting in better fatigue life relative to other welding techniques [5]. The Federal Aviation Administration (FAA) guidance and the Metallic Materials Properties Development and Standardization (MMPDS) databases provide validated design allowables for fatigue design of aluminum alloys, imparting sufficient confidence for engineering substantiation of fatigue design of aluminum alloys in aerospace

structures [6]. The introduction of hybrid materials systems, specifically aluminum alloys in combination with carbon fiber reinforced polymers (CFRPs), further intensifies complexity associated with stress compatibility and fatigue durability at the material interfaces, as there is a critical need to mitigate stress concentration at joints, often concerning the associated use of a compliant interlayer approach or shimming to reduce differential loading during fatigue to possibly enhance fatigue performance [7].

In summary, the evolution of aluminum alloys for aerospace applications has been driven by the need for higher strength, better fatigue performance, and lower weight. These developments have been enabled by alloy innovation, processing control, and structural design enhancements—all of which underpin the continued use of aluminum alloys in fatigue-critical aerospace components.

1.1.1. Stress Concentration and Fatigue Mechanisms in Aluminum Structures

Fatigue failure is a significant concern in aerospace structures, especially in components that experience cyclic loading. While aluminum alloys have better fatigue characteristics than steel, they are both still subject to fatigue crack initiation, particularly at locations with geometric discontinuities. Stress concentrations occur at geometric features (e.g., bolt holes, notches, or sudden changes in cross-sectional area) where the local intensity levels of the stresses exceed any nominal stress level. These stress concentrations are almost always where structural components will see the initiation and early propagation of fatigue cracks [8].

The most commonly used measure to represent the effects of the discontinuity along with the intensity of the defects or feature is the stress concentration factor (SCF). The SCF is defined as the ratio of the peak stress at the discontinuity to the nominal applied stress. In general, SCF values can differ significantly, depending on the geometry and loading mode of the feature. For example, a thin plate with a circular hole in the direction of tension will produce an SCF of approximately 3.0 in an ideal case. However, in real aerospace structures, SCFs can greatly exceed this due to compounded aspects of surface roughness, residual stress, or adverse loading conditions [9].

Aluminum alloys like 7075-T6, and 2024-T3, are very sensitive to micro-structural characteristics that impact fatigue behavior. Inclusions, inter-metallic particles, and precipitates of second phases can act as internal stress risers that facilitate fast crack nucleation. Environment also significantly degrades fatigue life through factors such as humidity, temperature variation, and exposure to corrosive conditions. Environment can make crack growth performance under multi-axial loading or spectrum loading even worse compared to uniaxial or constant loading [10].

Fatigue crack growth typically happens in two stages. The first stage is microstructurally short crack growth in the inter-granular and/or trans-granular on the slip band. The second stage of crack growth is longer and typically dominated by mode I crack growth across the crack width, perpendicular to the principal stress direction. Crack growth rates can typically be fitted to the Paris-Erdogan Law for most aluminum alloy, whereby crack growth rate shown in the log-log plot of crack growth rate versus the applied stress intensity factor range (ΔK), which for aluminum alloys, threshold crack growth rates are 2-5 MPa$\sqrt{m}$, varying by alloy compositions and surface quality [11].

Quantitatively describing SCFs and predicting fatigue behavior will be rooted in numerical methods, particularly finite element analysis (FEA). FEA is capable of providing substantial modelling of intricate geometries, load paths, and boundary conditions. In the numerical

simulation of crack initiation and propagation in an aluminum structure, extended FEM(XFEM) and cohesive zone modelling(CZM) are the most commonly used methods. Model validation of a FEA will often occur in the experimental test using digital image correlation(DIC), thermoelastic stress analysis(TSA), and strain gauges[12].

Methods to lessen the effects of stress concentrations on fatigue are available. Geometric design optimization, such as fillets, gradual changes in cross-section, and optimized fastener placement may reduce SCFs. Surface enhancement techniques, such as shot peening and laser shock peening may have beneficial compressive residual stresses which help delay crack initiation. For example, in aerospace uses, laser peening has been shown to increase the fatigue life of 7075-T6 by over 30%[13].

In conclusion, fatigue behavior in aluminum alloy structures is intricately linked to stress concentration phenomena, microstructural characteristics, and environmental influences. Understanding and managing these factors through modeling and design mitigation techniques is essential for ensuring long-term structural integrity in fatigue-critical aerospace components.

1.1.2 Shimming Techniques in Aerospace Structures

In the aerospace assembly sector it is common for mating parts to have unintentional gaps or misalignments with due to very small tolerances and complex geometries. Shimming is a useful technique to compensate for these conditions in order to achieve full contact and equally transfer load across the interfaces. A shim is a thin layer of material of precise size and shape that is inserted in between structural elements to make small corrections while keeping the structural integrity and alignment of an assembly intact. Traditionally, shimming was used to create physical offsets in geometrical compensation, yet more recently shimming has been utilized to elongate performance by reducing fatigue, redistributing stress, and sometimes to support limiting interface failure modes. In principle, the most common form of shimming would be a metallic shim (stainless steel, aluminum or titanium) which are used at high loads, they provide high stiffness and strength; however, once integrated into structural systems they produce significant localized stress concentrations due to the mismatch of stiffness in materials. Additionally, shimming utilizing dissimilar materials (like composites) could also create galvanic corrosion, when used with metal shims, making it unsuitable for hybrid structures and longevity [14].

Polymeric shims are more frequently being specified by engineers, manufacturers and repairers for their conformability to design and chemical resistance. Two of the plastics PTFE and polyimides are able to reduce the stress concentrations at the adhesive interfaces, however their usefulness as shim materials are rather limited in their degradation under specific conditions, creep and relatively low tensile strength under cyclic loading. More recently, researchers have explored epoxy resin shims which upon curing are much more conformable than other thermosetting adhesive shims and will provide a compromise between adhesion strength and conformability and could either be a pre-cured solid shim or a paste adhesive shim curing in place to provide a custom load bearing interface [15].

Epoxy resin shims have good resistance to solvents and hydraulic fluids at elevated temperature as well makes them as an option in military and commercial aerospace applications. Because they can be viscoelastic, epoxy shims also provide an opportunity to be dampers or crack arresters where cyclic or impact loading is likely. There are studies to suggest epoxy resin shims

influence the distribution of interfacial stresses at bonded joints as well as bolted joints, and have been shown to reduce the initiation.

Recent findings in the use of finite element analysis of structural joints have validated the positive effects of epoxy shims/laminates. Modeling of both shimmed and un-shimmed configurations with crack-like stress-concentration revealed a lower interfacial stresses and more uniform stress fields with compliant shim layers, thus yielding greater damage tolerance and a delayed crack initiation under cyclic loading [16].

In aerospace manufacturing, epoxy-based shimming has follow-out protocols practiced in a variety of applications, including fuselage assembly and wing-box assembly. Aircraft manufacturers, such as Boeing and Airbus, engage in controlled shimming at the final assembly phase that is standardized and formally controlled, to meet geometric fit-up, load path continuity, and other requirements. Conventional detached epoxy shims, and uses of epoxy shims in automotive manufacture that often includes bonding systems, are usually combined (i.e. use as filler and adhesive) to create a more consistent and reliable joint as a result of greater area of bond, as bonding is not an airtight process and produces fewer results of any other bond development. Studies have even noted the documented use of functionalizing a particular epoxy system (e.g. epoxies populated or reinforced with carbon nanotube (CNT) or graphene oxide) into shimming systems designed for mechanical strength, electrical conductivity, and thermal interface stability in designs. As well there are testable proofs of concept potential for multifunctional shims to provide standardized, components of integrated sensing or damage monitoring to new aerospace structures [17].

In summary, shimming has evolved from a dimensional adjustment tool to a functional design element in aerospace structures. The application of epoxy resin shims, in particular, provides a proven means to improve fatigue performance, reduce stress concentrations, and ensure structural reliability at critical joints.

1.1.3 Fatigue Performance Enhancement Using Epoxy Resin Shims

Fatigue is a predominant mode of failure in aerospace structures due to repeated cyclic loading encountered in service. Components constructed of aluminum alloys are light weight and structurally efficient; however, they are at risk of fatigue damage especially in areas with a geometric discontinuity, or high stress concentration. Regarding this concern, epoxy resin shims have long been recognized as potential contributors to fatigue performance at mechanical joints, but as gap-fillers or alignment shims. Fatigue cracks in bolted of riveted joints develop near fastener holes due to stress corrosion cracking that occurs from localized stress concentrations and micro-movements at the joints interface. The addition of an epoxy resin Shim imposed a compliant interlayer which redistributed the applied in such a way as to achieve more uniform stresses along the contact surface by smaller peak stresses. This experimental research demonstrated that epoxy shims added to mechanically fastened aluminum joints, offered increased fatigue life by delaying crack initiation and by reducing crack propagation under cyclic load.

Epoxy resins can positively impact fatigue life in three specific ways, namely stress redistribution due to compliance, dissipation of interfacial energy, and suppression of fretting fatigue. The reason for the stress redistribution is that the epoxy can deform slightly, which reduces local stress spikes where the fasteners are applied. At the same time, the viscoelastic nature of epoxy materials allow them to dissipate energy partially, which leads to a lesser driving

force for cracks to nucleate. When the epoxy shims are applied, they also lessen movement between contacting surfaces and lessen wear and surface damage, which can eliminate fretting fatigue a common predicament in bolted joints [18].

There is numerical evidence in finite element modeling to support this, as the simulations indicated up to 25% reductions in maximum interfacial stresses going from an unshimmed to a shimmed state due to using compliant epoxy layers. This allows the stress distribution to be more homogeneous and better fatigue life of the whole joint under cyclic loading. Specifically, the study showed that energy storing and dissipating potential of epoxy materials led to some strain energy being absorbed in the context of cyclic loading and also noticed that there was a measurable reduction of the J-integral close to the possible nucleation sites [19].

When optimizing fatigue behavior in epoxy shims, this means material formulation is an essential driver for performance. Crosslink density, type of filler, and curing conditions will influence mechanical properties, such as toughness, modulus, and fracture resistance. Work has indicated that epoxy shims with moderate stiffness and high fracture toughness provide the optimal balance between load transfer capability and energy dissipation. A high crosslink density can deliver high stiffness, but will not extend crack energy absorption as opposed to lower crosslinking, which improves ductility at the expense of overall strength [20].
Efforts to improve the performance of epoxies have also seen the addition of nano-fillers such as carbon nanotubes (CNTs), graphene nanoplatelets, and silica particulates. These reinforcements have improved interfacial bonding, thermal conductivity, and fatigue resistance. The experimental results suggest that CNT- reinforced epoxy composites improve resistance to fatigue crack growth and stiffness degradation with time, and therefore can be used in critical aerospace applications [21].

In addition, the long-term confidence to be placed in epoxy shims under aerospace environments has been demonstrated in previous research through environmental testing. The mechanical properties of aerospace-grade epoxies do not significantly degrade over service life from exposure to hydraulic fluids, thermal cycling, and UV exposure. Therefore, epoxy products maintain their strength command in both external and internal structures on an aircraft that are exposed to varying and extreme conditions in operation. [22]

In conclusion, epoxy resin shims do more than fill dimensional gaps—they actively contribute to the fatigue resistance and durability of aerospace joints. Their ability to redistribute stress, absorb strain energy, and mitigate micro-damage under cyclic loading positions them as a multifunctional solution in fatigue-critical aerospace structures.

1.2 Project Objectives

This project, therefore, seeks to:

- To assess fatigue performance for aluminum alloy structures with and without epoxy resin shims by finite element analysis (FEA).
- To simulate cyclical load conditions and assess the impact loading conditions have on stress, strain, deformation, and fatigue life of each configuration.
- To evaluate the effectiveness of epoxy resin shims to relieve stress concentrations and enhance fatigue resistance.
- To establish if shims improve the structural durability and reliability of aluminum alloy components under cyclic and repetitive loading conditions.

1.3 Methodology

The methodology for the project was to advance knowledge of the fatigue performance for aluminum alloy structures with and without epoxy resin shims by finite element analysis (FEA) with ANSYS Workbench 19.2. The purpose was to model the loading conditions, obtain the structural response parameters of stress, strain, and deformation and to participate in strain-life based fatigue analysis to observe the impact of shimming on fatigue life.

- Geometry Modeling

Two separate three dimensional models were created, one for the monolithic aluminum product, and one with a shim of epoxy resin between the two aluminum components. The geometry was modeled to ensure the same dimensions specifications for consistency to ensure that it would be possible to directly compare the two configurations. The geometry with the shim was modified locally to accommodate the shim region, while the rest of the geometry remained identical.

- Material Specification

The properties of the material were based upon published literature values and standard database values available. The mechanical properties of the aluminum alloy presented in both configurations were based upon the known properties, including Young's modulus, Poisson's ratio, yield strength, and ultimate tensile strength. The shim conditioned model had an epoxy resin material defined distinctly, with the elastic modulus, Poisson's ratio and the fatigue properties defined.

- Boundary Conditions and Loading

Fixed supports were assigned at one face of the component to prevent all movement. The vertical cyclic load, simulated loading during operational conditions, was applied with an additional pressure based loading on another face to replicate the distribution of the service like stresses. The loading conditions were consistent through each model to eliminate the variation of the shim on structural behavior and fatigue behavior.

- Mesh Study and Mesh Convergence

A mesh convergence study was conducted to help ensure accuracy in results without the excessive computing time and processing costs. Different mesh refinements were applied, and values for deformation, stress and strain were tracked at key locations on both configurations. The most optimal mesh was chosen based on the convergence of the three key variables and used in the fatigue analysis in the final portion of the project.

- Structural Analysis

Before conducting the fatigue assessment, a structural statics assessment was conducted for the two configurations to determine the key response parameters of total deformation, von Mises stress and equivalent elastic strain. The structural analysis revealed the deviation and strain distribution behaviour of, and areas of stress concentration that were useful for the fatigue simulation.

- Fatigue Analysis

Fatigue life prediction used the strain-life (ε–N) method for the ANSYS Workbench. The fatigue properties were defined for the aluminum and epoxy resin materials. The Morrow mean stress correction model was selected so that the mean stresses could be evaluated during the cyclic loading process. The solver was configured to include fatigue life, fatigue damage and safety factor contour calculations.

- Comparative Analysis

The structural assessment and fatigue assessment results for the shimmed and non-shimmed geometries were compared. The comparison considered the differences in stress distribution, total deformation behaviour and fatigue predictions. The results enabled an assessment of the relative improvement in the fatigue life of the composite part and the relative reduction of stress concentrations of the epoxy resin shim.

II. Finite Element Method

The Finite Element Method (FEM) is established as an essential computational analysis tool in engineering. FEM breaks down complicated geometries to discretize them into finite elements, allowing for the in-depth analysis of how structures behave under applied loads (these also include break load and each load path). FEM can evaluate stress distributions, deformations, and strain in very complicated structural components with complex geometries and materials. In many aerospace applications, such as the pressurized fuselage design of the Boeing 787, FEM was critical for assessing stress redistribution on the fuselage from structural features, such as shims, and effects from cyclic loading.

Besides structural analysis, FEM is also quite powerful in thermal analyses, fluid dynamics, and electromagnetic simulations. This versatility allows engineers to assess various design scenarios comprehensively without relying on building physical prototypes in the initial stages. With optimization refinement and an analytical examination of forces and loading conditions, engineers are capable of predicting system behavior and making informed decisions about design changes. This computational approach has fundamentally changed the way the design process in engineering is carried out. It substantially reduces the number of physical prototypes needed while improving the understanding of complex structural behaviors.

In the case of the Boeing 787 composite fuselage, the combination of advanced material science with sophisticated FEM analysis enables engineers to optimize both aircraft assembly practices and maintenance protocols. This coupling of materials design and analytical methods represents the very state of the art in aerospace engineering, wherein theoretical understanding and practical application meld to create safer, more efficient aircraft structures.
The equations underpinning FEM stem from the fundamental principles of physics, such as equilibrium, compatibility, and constitutive relations.
For structural mechanics, the equilibrium equation ensures that the internal stresses and external forces are balanced within the body:

$$\nabla \sigma + \{\vec{F}\} = 0 \qquad (2.1)$$

Here, σ represents the stress tensor, and F represents external forces such as gravity or applied loads.
The strain-displacement relation links deformations to strains:

$$\epsilon = \nabla \{\vec{u}\} \qquad (2.2)$$

Where ϵ is the strain tensor, and u is the displacement vector.
Finally, the constitutive equation defines the material behavior. For linearly elastic materials, Hooke's law is often used:

$$\sigma = C \cdot \epsilon \qquad (2.3)$$

Where C is the stiffness matrix which connects the strain tensor to the stress tensor.

In modern engineering, the need for optimized structural designs has intensified as industries strive for lighter, stronger, and more cost-effective solutions. Materials like Aluminum Alloy are widely used due to their excellent strength-to-weight ratio, corrosion resistance, and machinability. However, the growing complexity of engineering applications often necessitates the use of composite assemblies that combine multiple materials to achieve desired properties. These assemblies provide an opportunity to tailor mechanical behavior by strategically leveraging the strengths of different materials, enhancing overall performance while addressing

specific challenges such as weight reduction or thermal stability. Finite element analysis has become an indispensable tool for evaluating structural performance, enabling engineers to simulate real-world conditions with high accuracy. Advanced simulation software like ANSYS facilitates the modeling of complex geometries, the assignment of material properties, and the application of realistic boundary conditions. By employing FEA, engineers can predict potential failure points, validate designs, and identify opportunities for optimization before physical prototypes are created, saving time and resources. This study builds on these principles by investigating the structural behavior of a single component and a composite assembly under identical static loading scenarios. The single component, constructed entirely of Aluminum Alloy, serves as a baseline for comparison, offering a straightforward design with uniform material properties. The composite assembly, on the other hand, introduces complexity with its multi-material composition, aiming to demonstrate the advantages of combining materials to improve load distribution and structural integrity. The analysis methodology encompasses key steps such as geometry definition, material assignment, meshing, and the application of loads and boundary conditions. Results from the simulations, including total deformation, von Mises stress, and equivalent elastic strain, provide valuable insights into the mechanical performance of both models. The findings not only validate the designs but also highlight areas for improvement, offering recommendations for enhancing durability and safety. In addition to assessing structural integrity, this study contributes to the broader understanding of how material selection, geometric configuration, and meshing strategies influence mechanical behavior. The comparative approach underscores the trade-offs between simplicity and adaptability, offering guidance for engineers tasked with designing components for diverse applications. The results of this study have practical implications for industries such as aerospace, automotive, and civil engineering, where lightweight, high-strength designs are paramount. By evaluating the strengths and limitations of single-material and composite designs, this research aims to inform future development efforts, paving the way for innovative and efficient engineering solutions.

The Finite Element Method is a powerful numerical tool whereby engineers and scientists can adequately model complex engineered and scientific problems, which are too difficult or even impossible for analytical solutions. The advent of this technique revolutionized the way engineers and scientists approach problem-solving across all engineering and scientific disciplines, from structural analysis to heat transfer, fluid dynamics, and electromagnetics.

2.1 Basic Concepts and the Discretization Process

The concept which forms the heart of FEM is discretization. This is the process of partitioning the complex system or domain into small, manageable parts, known as a finite number of elements. The elements themselves are held together at discrete points called nodes; this configuration together is termed a mesh.

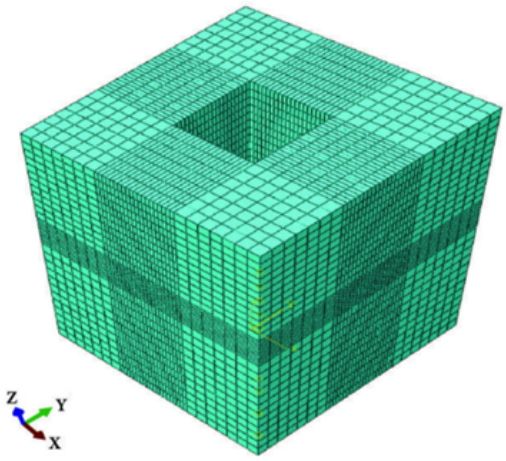

Figure 1- Schematic of a finite element mesh.
[23]

Figure 1 demonstrates the discretization process applied to a 3D solid geometry using the finite element method. The model is divided into smaller subdomains called elements, shown here as structured hexahedral (brick) elements. These elements are connected at their vertices and edges through nodes, forming a continuous mesh across the domain. This meshing enables numerical approximation of the governing field equations, providing detailed insight into structural behavior under loading

Let us take an example to explain the process of discretization. Consider a simple problem beam subjected to a distributed load.

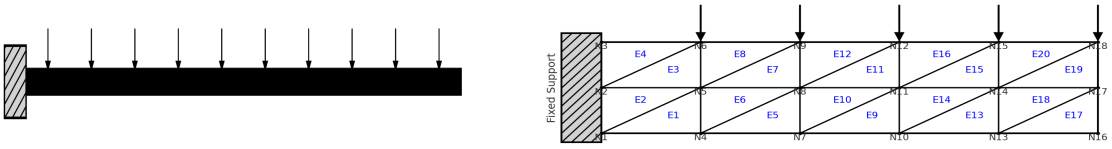

Figure 2- Discretization of a cantilever beam subjected to a distributed load.

1. The first step is to discretize the beam; divide it into several smaller parts (elements)(Elements are denoted by E).
2. Each element is defined by the nodes on its endpoints (Nodes are denoted by N).
3. A simple trial function (called the shape functions) describes the displacement field in each element.
4. The total response of the beam, subjected to the loading, is described by this assemblage of element behaviors.

This discretization allows for such complex geometries to be approximated by a constellation of simple shapes, such as triangles or quadrilaterals in 2D and tetrahedra or hexahedra in 3D.

2.2 Types of Elements and Their Formulation

FEM analysis has elements that are known as the building blocks of the analysis. There is more than one basic type of element available for use, and the suitable element selection depends on how accurately the numeric solution is needed and the structural application of the element.

- The linear element is the basic first-order (linear) interpolation between the nodes of the element to approximation of the displacement field. The linear element is computationally fast to run and is generally suitable for problems where stress gradients are not large. However, in the areas of high geometric complexity and/or curvature, the linear element would be less accurate unless a very fine mesh is defined.
- Quadratic elements utilize a second-order polynomial that includes mid-side nodes as well as corner nodes to interpolate and capture curved geometries and variable stresses in an element. Because of the increased accuracy, they are effective where detail is needed, but with no significant increase in total elements.
- Shell elements are best used for structures that are thin-walled in order of magnitude with respect to the other two sizes. A shell element accounts for both bending and membrane behaviours. Shell elements are likely the best choice for representations of most aerospace elements such as fuselage skins, wing surfaces, and stiffened panels. It allows for modelling fatigue behaviour and accuracy in thin structures with minimal computational effort.
- Solid elements, also referred to as 3D or brick elements, are used to model thick or volumetric structures. In contrast to shell elements, solid elements can take into account stress variation throughout the entire body, including through the thickness. In this project solid elements were useful for modeling the shimmed and non-shimmed equivalent aluminum alloy geometries allowing for a comprehensive evaluation of deformation, stress concentration, and fatigue behaviour in response to cyclic loading. Solid elements can be more practical when modelling joints, interfaces or assemblies with multiple materials, such as with epoxy resin shims.

The way field variables, such as displacement or stress, are interpolated inside each element affects the performance and accuracy of these element types. This interpolation is carried out using shape functions, which are mathematical tools that define how values like displacement vary within an element. These shape functions differ for linear, quadratic, or higher-order elements, depending on how accurately the variation needs to be captured.

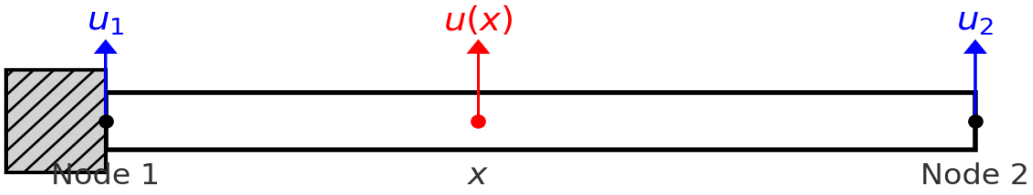

Figure 3- Displacement interpolation in a cantilever beam.

For example, in a one-dimensional linear element with two nodes, the displacement u(x) at any point within the element can be approximated as:

$$u(x) = N_1(x)u_1 + N_2(x)u_2 \quad (2.4)$$

Where N_1 and N_2 are shape functions, and u1 and u2 are nodal displacements.

To understand this intuitively, consider a cantilever beam fixed at one end and free at the other, as shown in figure 3. If we model this beam using just two nodes one at the fixed end and one at the free end we can compute how any point in between those nodes moves using the shape functions. These functions act like a smart weighting system: the closer a point is to Node 1, the more influence u_1 has; the closer it is to Node 2, the more it depends on u_2. This results in a smooth and continuous estimate of displacement throughout the beam.

2.3 Types of Solutions and Problem-Specific Approaches

FEM solutions vary with the problem type and phenomena to be modeled:

- Static analysis to solve equilibrium conditions under constant loads.
- Dynamic analysis accounting for time-dependent effects and inertial forces.
- Linear analysis which assumes small deformations and linear behaviour of the material.
- Nonlinear analysis, which considers large deformations, material nonlinearity, or contact problems.
- Steady-state heat transfer is used to solve for distributions of temperatures in thermal equilibrium.
- Transient analyses, which solve time-dependent problems of heat propagation and vibrations.

In this context, solution type can largely influence the problem formulation and computational approach: Static structural analysis may be described by simple linear equations, while a non-linear dynamic analysis would likely require iterative solution algorithms with time-stepping.

2.4 Advanced Techniques and Applications

Several advanced techniques for different applications in FEM have arisen since its inception.

- Adaptive Mesh Refinement (AMR): Self-reforming mesh that improves accuracy in areas where the solution gradient is higher.
- Extension of the finite-element method (XFEM): Methods that allow cracks and interfaces to be modeled without remeshing using rich, discontinuous enrichment functions.
- Multiphysics coupling: Formulation techniques that allow simultaneous analysis of different physical phenomena (for example, fluid-structure interaction or thermo-mechanical problems).

FEM is a widely used and used software in several sectors:

- Aerospace: Aircraft component structural analysis, aerodynamic simulations.
- Automotive: Crash simulations, noise and vibration analysis, thermal management.
- Civil Engineering: Structural analysis of buildings and bridges, along with studies of seismic response.
- Biomedical Engineering: Modeling of prosthetics and analysis of blood flow and tissue mechanics.
- Electronics: Thermal Management of Electronic Components, Electromagnetic Simulations.

2.5 Limitations and Considerations

While a powerful tool, FEM does have limitations of which users should be aware. The following should be considered.

- Solution accuracy is dependent on mesh quality and element formulation.
- Understanding the underlying physics is necessary to interpret results properly.
- Fatigue analysis using fine meshes and strain-life methods can become computationally intensive, especially when working with detailed 3D geometries, or involving several load cycles.
- Some phenomena, such as fractures and large deformations, may require specialized techniques for modeling.

III. Geometry, Materials, and Loading Conditions

This chapter will describe the geometric configurations, material assignments, load conditions, and mesh convergence strategy used in the finite element analysis of the aluminum alloy component, with and without epoxy resin shims. It includes comparisons where two models were created, one a monolithic aluminum alloy structure and the other a shim interface where a shim of epoxy resin replaces a section of aluminum alloy. The properties for the aluminum alloy and epoxy resin were developed using materials properties references and fatigue data. Loading and boundary conditions were used to define favorable simulations of service environments, allowing a full evaluation of stress distributions, deformations, and fatigue life in that service environment. A mesh convergence study was determined to verify the simulation accuracy was independent of mesh size and was numerically stable.

3.1 Geometry without shim.

The metal component is modeled as a three-dimensional solid body with dimensions measuring 150 mm along the length (X-direction), 18 mm along the width (Y-direction), and 50 mm in height (Z-direction), which corresponds to a volume of 5.349 x 10^{-5} m^3 with a mass of 0.14817 kg. The geometry is shown in Figure 4. Aluminum Alloy has been selected in this analysis for its excellent strength-to-weight ratio and common use in engineering applications. The material properties are listed in Table 1.

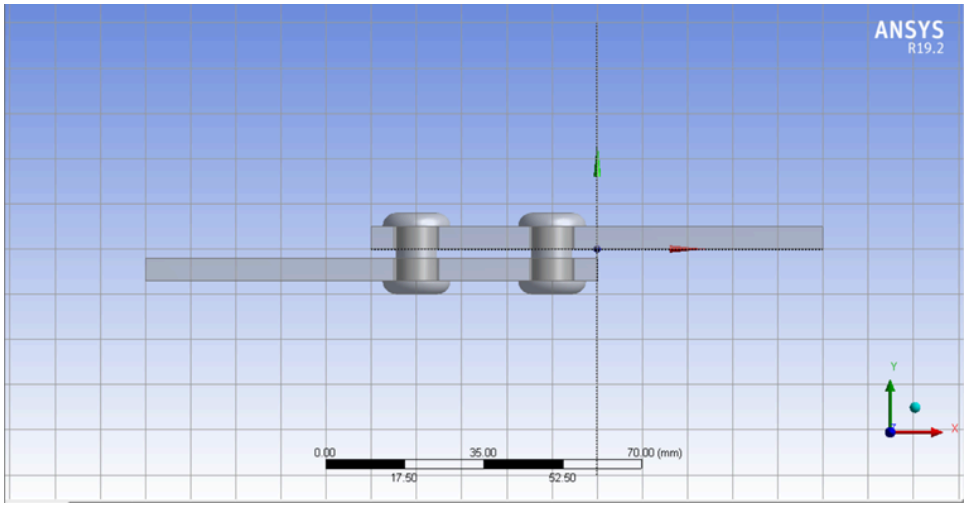

Figure 4- Geometry of component without shim

Table 1: Material properties of Aluminum Alloy

Particulars	**Unit**
Density	2770 kg/m^3
Young's Modulus	71 GPa
Poisson's Ratio	0.33
Tensile Yield Strength	280 MPa
Tensile Ultimate Strength	310 MPa

3.2 Geometry with shim.

The composite assembly model, shown in Figure 5, considers epoxy resin shimming, resulting in a modified geometry. The dimensions of the assembly model are consistent with those of the single component, measuring 150 mm in the length X-direction, 18 mm in width Y-direction, and 50 mm in height Z-direction. But given the shimming, the character of the component drastically changes:

- Total volume: $5.7862 \times 10^{-5}\ m^3$
- Mass: 0.15324 kg

The interaction of those units in a concocted form establishes multicentric attributes, one of the best examples of a heterogeneous body in the resin, allowing flexibility in certain local regions, depicted in Figure 5. With this high contrast in stiffness between materials, starting from Young's Modulus values of 71 GPa and 3.78 GPa, respectively, it is expected that the stress concentration and deformation behavior for the composite assembly would change. The material properties of Epoxy Resin are listed in Table no 2.

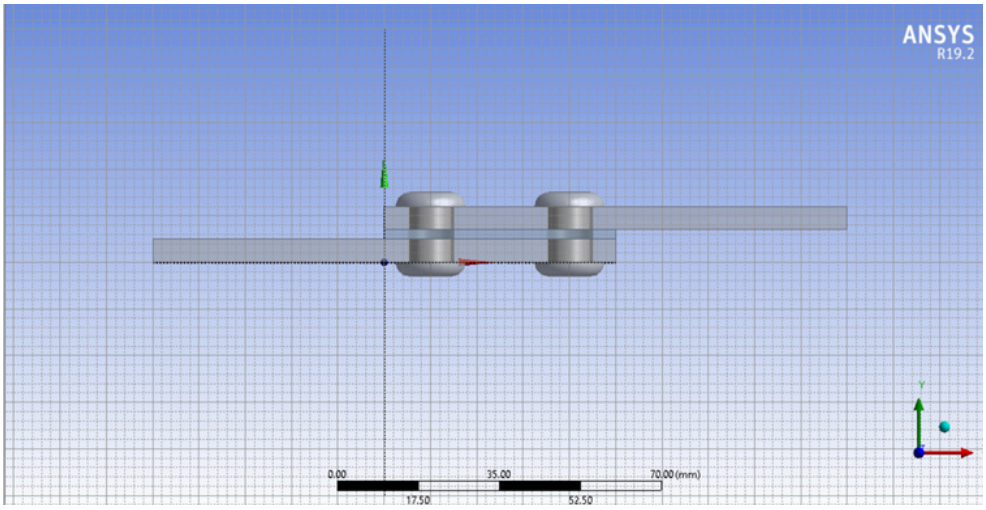

Figure 5- Geometry of component with Epoxy Resin

Table 2: Material properties of Epoxy Resin.

Particulars	Units
Density	1160 kg/m
Young's Modulus	3.78 GPa
Tensile Yield Strength	54.6 MPa

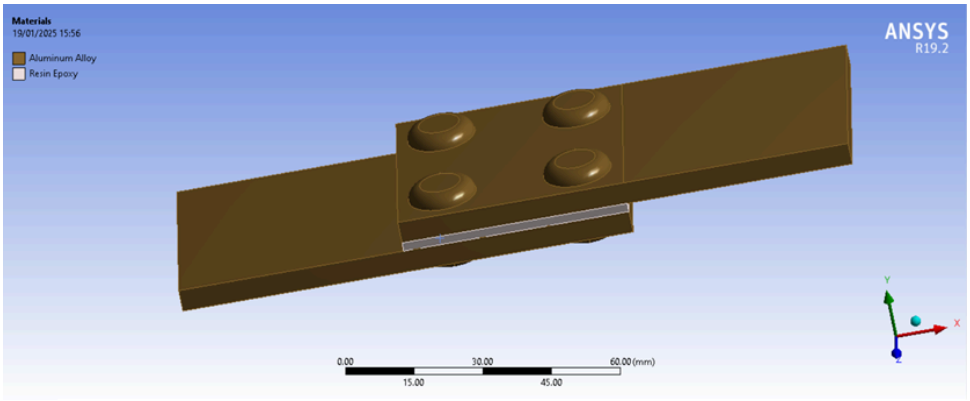

Figure 6- Material distribution on component with Epoxy Resin

3.3 Boundary Conditions and Loads without Shim

The loading conditions chosen for this project are based on simplified assumptions that typically appear in academic studies and as preliminary design-level studies of aerospace components. The vertical force of 1500 N approximates the load due to the weight or the combined forces of mounting small- to medium-sized aluminum structures, and is consistent with the common assumptions of static structural analysis. The added horizontal force of 300 N was included to capture the effect of secondary shear forces potentially resulting from operational misalignments or possible lateral load paths through the actual joint configurations. Both values similarly fall within the forces seen in typical aerospace simulation studies that included structural loading [24].

A cabin pressure of 50,000 Pa (0.5 bar) was chosen as a scaled value from standard fuselage pressurization conditions in commercial aircraft that are about 0.75 bar (75,000 Pa). The scaled pressure value permits computational convenience at the expense of producing an accurate mechanical representation of internal pressure loads for use in stress analysis [25].

In the model, these loads were ramped up to prevent numerical instability during the loading phase and better simulate real loading conditions.

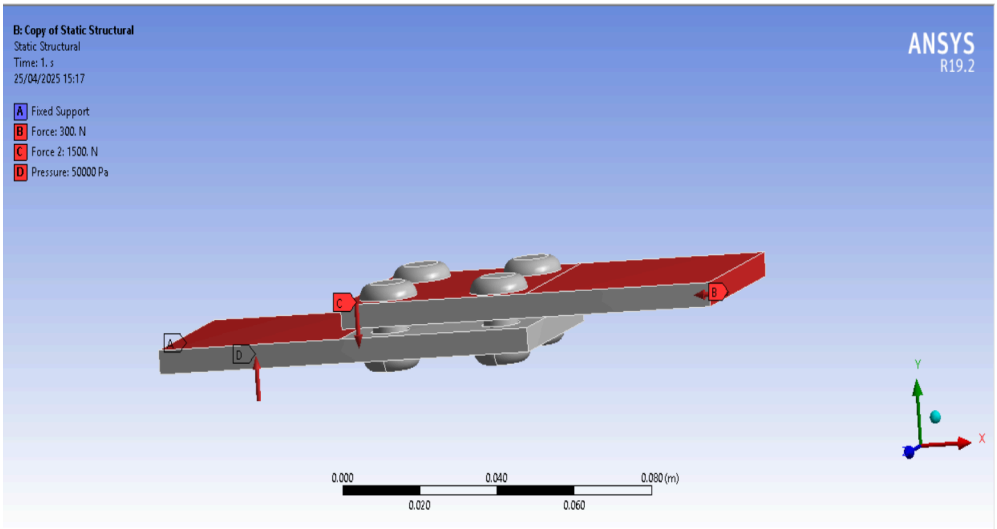

Figure 7- Boundary conditions and loads for the component without a shim

3.4 Boundary Conditions and Loads with Shim

Loading and boundary conditions applied to the composite assembly, as demonstrated in Figure 8, were identical to those used in the single-component test to facilitate direct comparisons between results:

- Fixed support: Applied to one face of the model, constraining all degrees of freedom.
- Vertical force: 1500 N
- Horizontal Force: 300 N
- Cabin pressure: 50000 Pa distributed across specific surfaces.

These conditions imitate real-world application scenarios, allowing the analysis of the shimming effect on the structural behavior of the component in the loaded condition.

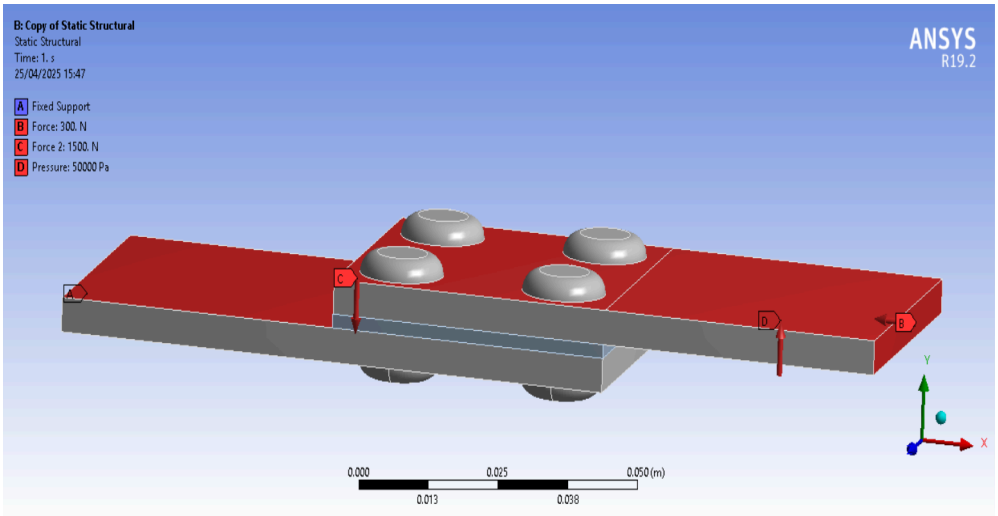

Figure 8- Boundary conditions and loads for the component with Epoxy Resin

3.5 Mesh Convergence.

3.5.1 Introduction

Mesh convergence represents an important process in Finite Element Analysis (FEA) to ensure the numerical results are accurate and reliable. Finite Element Analysis is defined as a process in which the structure is broken down into small elements, named a mesh. The accuracy of the solution is dependent on the size and quality of the mesh, with the trade-off being that finer meshes require a higher computational cost. The purpose of the mesh convergence study is to determine the appropriate mesh size for an optimal balance of accuracy and expertise. The mesh convergence is achieved when the mesh refinement does not significantly affect the results of the parameters of interest, such as deformation, stress, or strain. Mesh conversion is important because using a too coarse mesh can lead to incorrect or inappropriate results, while an excessively fine mesh causes unnecessary computational costs. Mesh convergence occurs when the numerical solution approaches the theoretical or experimental value within an acceptable range of the target value. In this study, we follow this process by refining the mesh and analyzing the effects on deformation, stress, and strain. A mesh convergence study often involves looking at the rate of convergence of a solution variable (e.g, stress σ, or a displacement u) as the mesh refines, and can be assessed statistically by the following relation:

$$E_n = \frac{|Q_n - Q_{n-1}|}{|Q_{n-1}|} \times 100 \quad (3.1)$$

Where:

- E_n = Percent error between two successive mesh refinements
- Q_n = Computed value (stress, strain, deformation) for current mesh size
- Q_{n-1} = Computed value for the previous mesh size

The solution is said to be converged when E_n falls below a predefined threshold (typically 1–5%) [27].

3.5.1.1 Importance:

The importance of mesh convergence is highlighted in multiple engineering applications:

- Ensures Accuracy: Without mesh convergence, FEA results may be misleading, leading to poor design decisions [28].
- Reduces Computational Cost: A fine mesh increases accuracy but can be computationally expensive, making convergence studies essential for optimizing resources [29].
- Validates FEA Models: Mesh convergence serves as a validation step, ensuring that the results are not an artifact of mesh resolution but reflect real physics [30].
- Prevents Over-Refinement: Without a convergence study, one might use an excessively fine mesh that increases solution time without significant accuracy improvement [31].

For example, in structural simulations, improper mesh selection can lead to underestimation of stress concentrations, which may result in unexpected failures in real-world applications [32].

3.5.1.2 Purpose:

This study aims to analyze the effect of mesh refinement on the deformation, stress, and strain results in a structural component. The specific goals are:

1. Determine the optimal mesh size where results stabilize.
2. Analyze deformation, stress, and strain using strategically placed probe points.
3. Compare "with shim" and "without shim" cases to understand their effect on structural behavior.

A shim is a thin piece of material used to adjust spacing or alignment. In this study, the presence of a shim affects stress distribution and stiffness of the component. Understanding how the mesh influences results with and without the shim will provide insights into the mechanical behavior of the system [33].

3.5.2 Probe Selection for Deformation, Stress, and Strain Analysis

To obtain a reliable representation of the mechanical response of the structure, specific points were chosen at which to extract deformation, stress and strain values from the finite element analysis. Point probes were chosen to be located in the critical zones where mechanical behaviors were expected to occur. The specific locations of points were selected based on stress concentration areas, notable deformation patterns, and strain value distribution to see a complete model response.

3.5.2.1 Probe Selection for Deformation Analysis

Deformation in finite element analysis takes into consideration both the boundary conditions and the consistently applied loads. Since we want to consider the deformation trend, the probe points can be seen in the corners of the free end of the structure in Figure 9. The placement of these points was significant as the free end would experience maximum displacement under the

applied loading conditions, while the opposite end of the free sample would be restrained and provide a point of reference for relative displacement values.

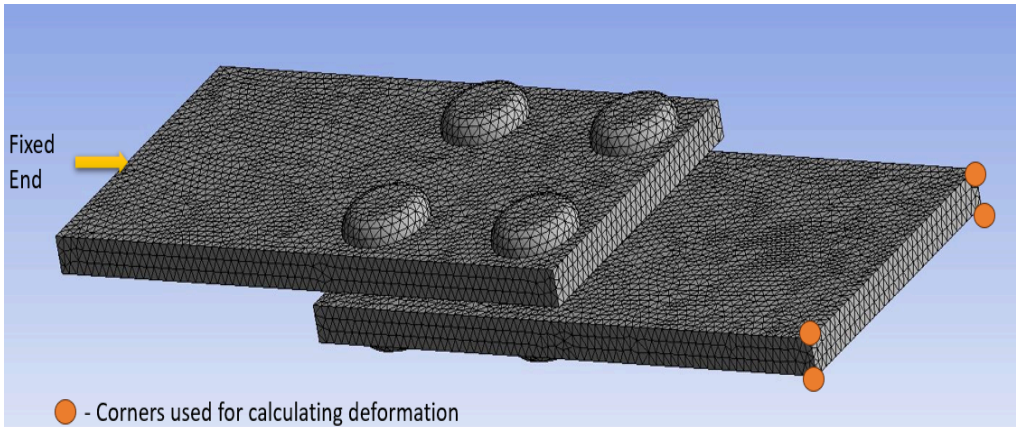

Figure 9- Probe selection for deformation

The deformation measuring points selected are favorable indicators of the structural formulation's flexural characterization. In structural mechanics, deformation consistently increases as the distance from the anchored end increases, which makes the free-end measuring corners suitable areas to span probes. Since the deformation across the selected measuring corners was sustained at several mesh refinements, the authors ensured that these observed values of displacement would not significantly change due to numerical error from mesh at coarser mesh. Measuring the deformation recorded at measuring probe points was achieved across several mesh sizes to observe convergence trends. Ideally, the deformation values would remain constant as the mesh is refined to achieve a converged solution. Any significant variations greater than a mesh size would signify the result of a converging solution that requires further refinement to overcome the discretization error.

3.5.2.2 Probe Selection for Stress Analysis

To conduct the stress analysis, probe points were allocated to areas of high stress concentration, primarily at the interfaces, locations of bolts, and significant load transfer locations. Stress concentrations are known to occur at locations where there is a discontinuity in geometry, either with holes, sharp corners, or contact. As identified in the structure under investigation, the fixed end was identified as one of the critical areas where it was expected that the stress values to be the highest. The probe points' stress values obtained in Figure 10 were analyzed too to verify that the mesh refinement process reported appropriate stress variances as intended. It is a known methodology in finite element analysis that stress values begin to deviate if the element mesh is too coarse (especially at sharp corners with a singularity). In systematically refining the mesh and capturing probe values at critical locations where we expect high stress induced, the study confirmed that converging values began to reach an asymptote.

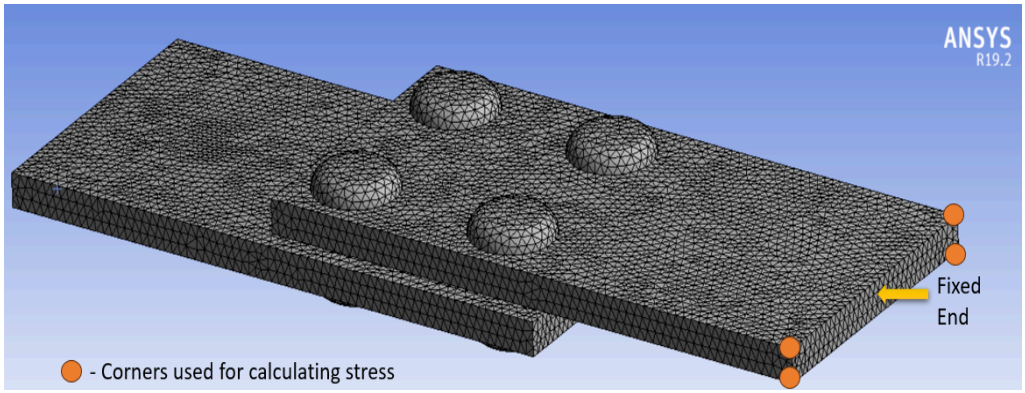

Figure 10 - Probe selection for stress

In addition, an average stress value was calculated from the selected probe points to reduce localized variability in stress estimates and to yield a more representative estimate of stress for evaluating the structural response. The stress convergence plot was subsequently inspected to confirm it tended toward the expected theoretical value asymptote.

3.5.2.3 Probe Selection for Strain Analysis

Likewise, for strain analysis, strain probe points were placed at locations showin in the figure 11.

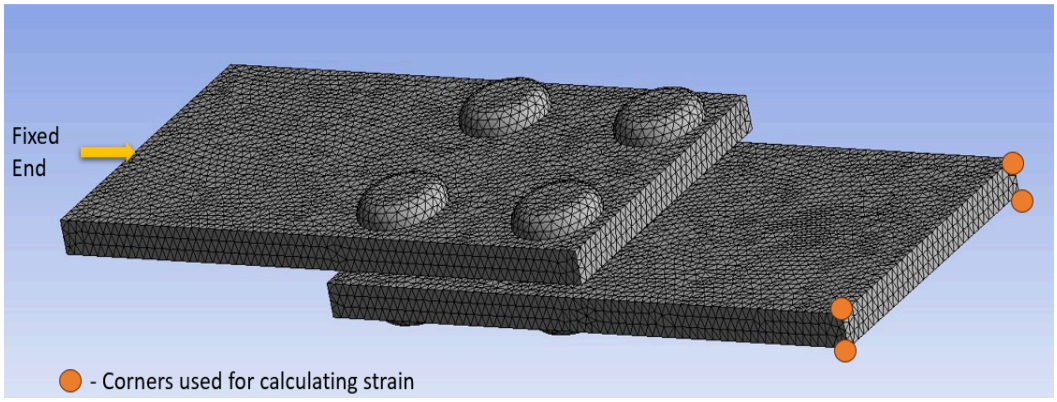

Figure 11 - Probe selection for strain

Strain values were taken over multiple mesh refinements to establish trends for convergence. With the relative sensitivity of strain values to both element distortion and irregularities in mesh, attention was paid to the quality of the elements at the probe location. An average strain value could then be estimated by taking the mean value of the strain from all probes that had been selected to gather strain at the probe points. This approach might have reduced the localized numerical variation and led to a more stable estimate of the strain.

3.5.2.4. Conclusion of the Probe Selection Strategy

The probe selection strategy followed in this study is in accordance with typical finite element analysis principles, where probes or strain gauges are placed in regions where it is deemed to be important to measure deformation, stress, and strain across differing refinements in the mesh. The data from the probes were used to generate convergence plots, which confirmed that the mesh refinement process resulted in the stability and accuracy of the numerical solution.

3.5.2.5. Interpretation of Results from Probe Analysis

After the probe locations were strategically chosen for the deformation, stress, and strain measurement of the study's structure, the next step was to interpret the numerical results from those points in order to assess the effects of the induction of the deformation on the accuracy and stability of the solution using different mesh sizes. By probing the information, we were able to gain additional insights into the mechanical response of the structure of interest. Results were compared, trends were established, and convergence was established for the purpose of verifying the numerical stability of the finite element analysis process. Tables 4 report the mesh sizes used to obtain the analysis, including element size, number of elements, and nodes.

Table 3: Mesh details for geometry with shim

Mesh	Element size (m)	Number of Elements	Number of nodes
A	0.004	12247	17138
B	0.002	49898	66846
C	0.0015	82743	112041
D	0.001	195020	262542

Table 4: Mesh details for geometry without shim

Mesh	Element Size (m)	Number of Elements	Number of Nodes
A	0.004	10042	15519
B	0.002	38684	57424
C	0.0015	69101	102160
D	0.001	163990	240938

3.5.3 Probe Analysis for Geometry without Shim

3.5.3.1 Deformation Analysis and Interpretation

The deformation results at each probe location were measured based on the mesh size, starting from the coarsest to the finest mesh. Generally, it can be stated that the deformational results became more consistent with increasing mesh refinement. The displacement values recorded on coarser meshes experienced larger oscillations, which is to be expected through averaging effects on element stiffness. Since larger elements will result in a lower resolution of displacement gradients, the resultant deformation may be overestimated. This was most obvious in the free end corners where maximum deformation occurred. Table 5 shows how the deformation results of different mesh sizes are compared, with percentage error as the convergence accuracy indicator.

Table 5: Deformation values for geometry without Shim

Mesh	Deformation (mm)	% Error
A	4.8086	0.97
B	4.84215	0.28
C	4.8486	0.15
D	4.8558	0

Concerning mesh refinement, the deformation values of the free end progressively increased to more converged values, as can be seen in Figure 12. The differences in deformation between consecutive mesh refinements became less and less, which indicated that the numerical solution was approaching the asymptotic limit. Experimental results showed that after a specific mesh

size, there was little noticeable difference in deformation as the mesh was refined; this indicates that a sufficiently accurate value has been determined.

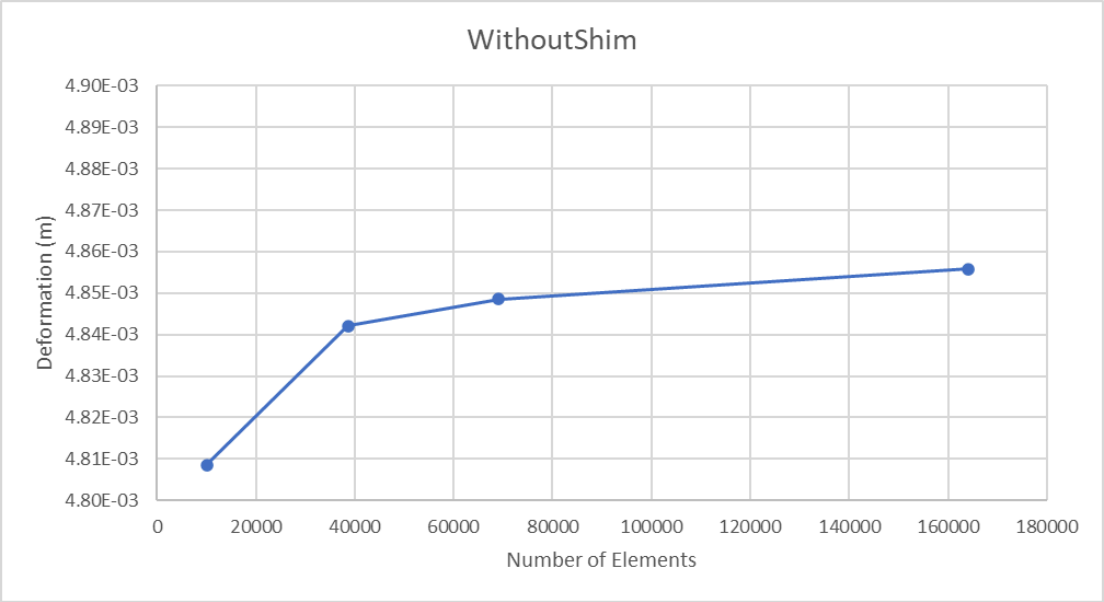

Figure 12: Graph representing deformation for geometry without shim

A mesh convergence plot was created to study deformation by plotting deformation values on the y-axis versus mesh size on the x-axis. The mesh convergence plot showed a monotonic convergence behavior with deformation values remaining stable as the element size decreased. At the finest mesh, the deformation values were nearly identical to the step before, implying that further mesh refinement would not enhance the solution but would increase computational cost and resources. This finding corroborated the theory of Finite Element Analysis, which states that deformation convergence typically occurs faster than stress convergence due to the fact that the mechanics are calculated from an integral.

3.5.3.2 Stress Analysis and Interpretation

The subsequent analysis focused on stress values that were determined from the probe locations that had been defined, and specifically concentrated on areas of elevated stress. The analysis showed that stress values were more sensitive to mesh density than deformation, which was most pronounced in regions around contact faces, the locations of bolts, and in the vicinity of other sharp edges, where high stress gradients existed. For example, the stress values, as interpreted from the probe location, were much lower than anticipated for a relatively coarse mesh due to the averaging of stress obtained from having an inadequate number of elements in the high-gradient regions where stress concentrations exist. As the mesh density increased, the stress values began to reflect higher values, as the mesh was able to appreciate the sharp stress variations by having more mesh points, as demonstrated in Figure 13. Notably, stress values did not show smooth convergence trends as did deformation; rather, there were greater fluctuations in stress convergence. This is well documented in finite element literature in that stress is a computed quantity that relies on displacement gradients, meaning that stress appears to experience more numerical instability when employing coarse meshes.

Table 6: Stress values for geometry without Shim

Mesh	Stress (MPa)	% Error
A	79.296	13.90
B	83.343	9.50
C	89.175	3.18
D	92.104	0

A notable feature of the stress analyses was the asymptotic behavior of the mesh convergence curve. Ideally, as the mesh is refined, stress values should converge to a theoretical limit. In some instances, the stress convergence curve would intersect the theoretical, asymptotic line, suggesting potential numerical artifactual or even numerical singularities. These instances were carefully examined to ensure that they were not due to mesh distortions of shape complications of the underlying elements, or even potential solver instability.

To assure the accuracy of the stress results, an average stress value was calculated by taking the mean of the stress values from multiple probe points. The average was taken to dampen the effect of localized variations around the probe point while giving a reasonable estimate of the stress distribution. The results demonstrated that stress values, after a given mesh size, had flatlined to a stable level, thereby indicating the solution had fully converged.

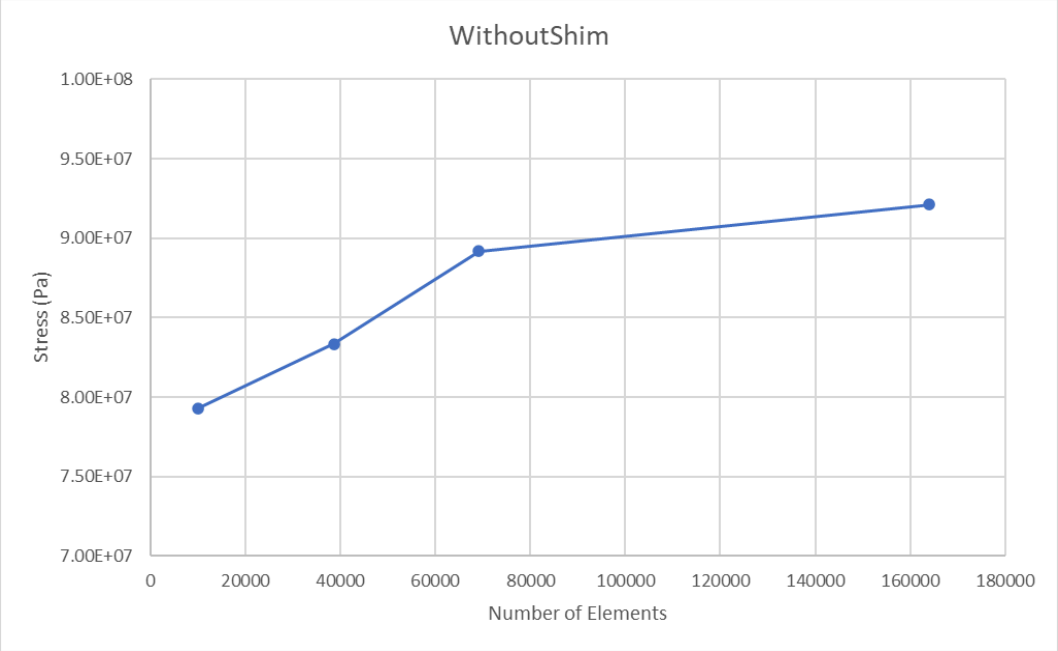

Figure 13: Graph representing stress for the geometry without the shim

3.5.3.3 Strain Analysis and Interpretation

The strain results followed a trend similar to stress but showed even greater sensitivity to mesh refinement. It is shown in Figure 14. Since strain is derived as the derivative of displacement, then translating variations that can happen in displacement can be enhanced in strain

calculations. That said, strain calculations were particularly sensitive in areas that endured localized deformation as a result of applied loads and boundary conditions.

Table 7: Strain values for geometry without Shim

Mesh	Strain (με)	% Error
A	4.2763	6.79
B	4.0138	0.24
C	4.0106	0.16
D	4.0041	0

In the coarsest configurations, strain values were extensively underestimated, which was simply due to the element resolution capability in areas of high strain gradients. As the mesh was refined, strain values continually increased until they approached a stable limit. Despite this, in certain instances, fluctuations persisted in strain values even amongst the relatively fine meshes. This behavior was likely due to element distortions, and/or numerical oscillations that can occur when using relatively high refinement levels, particularly when good reasoning can be used towards a highly localized concentration of strain.

In order to lessen the variation, a single strain value was calculated as the average strain for multiple probe locations, which lessened the impact of the localized variations and created more uniformity in the strain distribution estimate. The strain convergence plot exhibited a similar curve to the stress convergence plot. It began with deviation or fluctuation, but once interfering fluctuations began to become less prevalent, it came together and reached consistency and convergence with further mesh refinement.

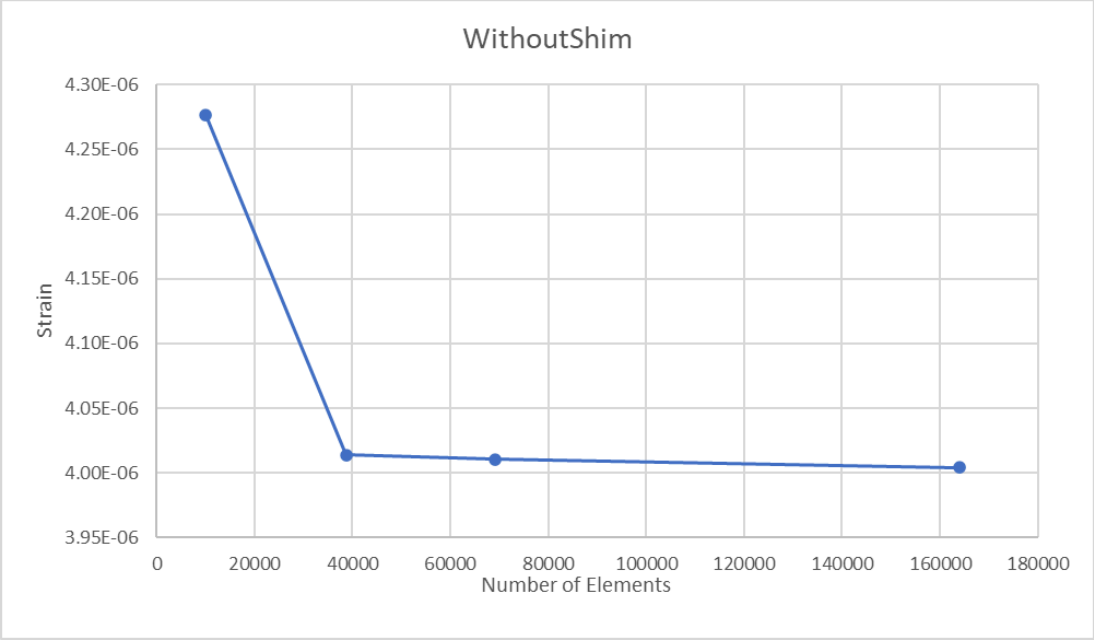

Figure 14: Graph representing strain for geometry without shim

One of the practical questions concerning strain analysis includes the necessity for appropriate elements in the refinement steps of the mesh, especially in locations that are experiencing large

strain gradients, and having elements that are poorly shaped in such locations may compromise a predictable strain and may contribute to some numerical issues. This study also ensured that those poorly shaped elements in high-strain areas had the lowest possible aspect ratio and minimal skewness, which all contributed to a more reliable outcome.

3.5.4. Probe Analysis for Geometry with Shim

3.5.4.1 Deformation Analysis and Interpretation

Plotting deformation values vs mesh size produced a mesh convergence plot for deformation. As the element size shrank, the deformation values stabilized, and the figure showed a monotone convergence trend. The deformation values, however, only slightly differed from the prior refining stage at the finest mesh level. This suggested that additional refinement would just raise computing costs rather than produce noticeable advantages. This observation was consistent with well-established finite element analysis principles, which state that because displacement computations are integral, deformation convergence typically happens more quickly than stress convergence. The deformation results for various mesh sizes are compared in Table 8, where the precision of convergence is shown by the percentage error.

Table 8: Deformation values for geometry with shim

Mesh	Deformation (mm)	% Error
A	4.5685	0.71
B	4.5931	0.17
C	4.5975	0.08
D	4.6011	0

The deformation values in Figure 15 seemed to grow incrementally with each subsequent mesh refinement, but they began to level off, approaching a more converged value. The numerical solution was approaching an asymptotic value and the deformation range again approached "0" for the difference between the successive (deformation) mesh refinements. The increased mesh refinement is showing the results were converging to an acceptable level since the deformation or maximum difference in the actual deformation hadn't changed appreciably as a range or wrt total number.

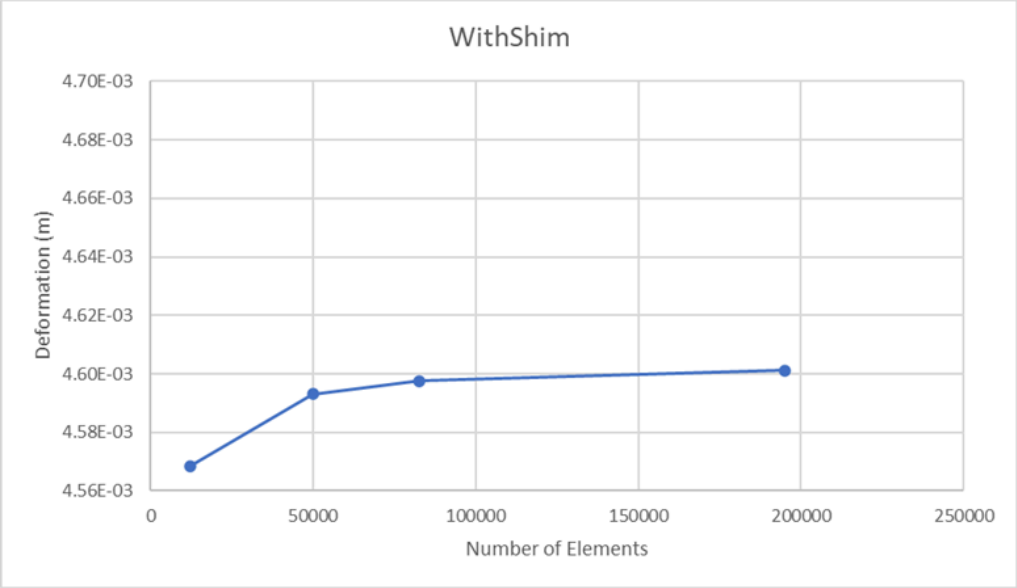

Figure 15: Graph representing deformation for geometry with shim

Deformation versus mesh size was plotted generating a mesh convergence plot for deformation, which exhibited a monotonic convergence trend and increasing stabilization as the element size decreased. However, at the finest mesh, the values for deformation were not meaningfully different from the previous refining stage and suggested that refinement would only increase computational demands without substantial benefit. This observation is aligned with the understood principles of finite element analysis, that is, since displacement values are computed as an integral, the convergence values are usually achieved at a faster rate for deformation as we move toward lower element sizes.

3.5.4.2 Stress Analysis and Interpretation

Subsequently, it became necessary to evaluate the stress values acquired from probe locations while identifying regions of high-stress accumulation. Results indicated that stress was more sensitive to the refinement of mesh than deformation. This effect was more prominent in regions of high-stress gradient, such as regions towards and in contact, bolt locations, and sharper geometrical locations. As a result of stress averaging due to the low element resolution in high-stress gradients, stress values in the coarse mesh were, in fact, lower than what could be anticipated. As mesh density increased, the stress readings began to increase, indicating the improved ability of the mesh to detect the abrupt stress transition (indicated in Figure 16). Stress convergence values varied more than deformation convergence, which bumped up against a consistency of convergence.

Table 9: Stress values for geometry with shim

Mesh	Stress (MPa)	% Error
A	52.29	47.67
B	86.508	13.43
C	95.605	4.32
D	99.927	0

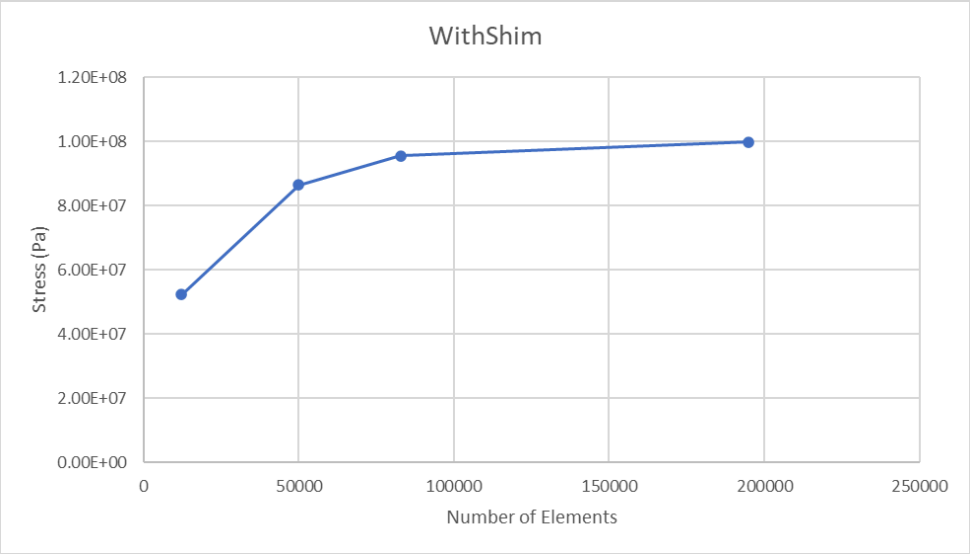

Figure 16: Graph representing stress for the geometry with shim

The asymptotic property of the mesh convergence curve was an important observation in the stress analysis. The stress value should ideally converge toward a theoretical value at finer meshes. The stress convergence curve, when plotted against the theoretical value, occasionally visited the predicted asymptotic line, which suggested that there were either some singularities in the solution, instability in the numerical computation. The research made sure to investigate these occurrences to avoid them being attributed to element shapes, mesh deformations, or solver issues. To ensure accuracy, an averaged stress value was computed by averaging the stress values from many probe locations. The averaged value minimized the effect of isolated variability and better approximated a value for the distribution of maximum bending stress. Results indicated that the program was converging once stress values stabilized for the refinement level.

3.5.4.3 Strain Analysis and Interpretation

While the strain results were even more mesh refinement sensitive, they also followed the same trend as the stress results. Figure 17 illustrates this. Any discrepancy in displacement estimates gets magnified in strain calculations since strain is calculated as the derivative of displacement. This sensitivity was most pronounced where applied loads and boundary conditions were causing localized deformation.

Table 10: Strain values for geometry with shim

Mesh	Strain (με)	% Error
A	4.6922	0.05
B	4.7758	1.83
C	4.7289	0.83
D	4.6898	0

Due to the absence of element resolution in regions of high strain gradients, values of strain were severely underestimated in the coarsest mesh configurations. As the mesh was refined progressively, strain values increased and converged towards a limiting value. To dampen these

oscillations, an average value of strain was achieved by taking the mean strain at a number of probe points. This approach gave a more stable determination of the distribution of strain while reducing, at the same time, the influence of localized anomalies. Like stress, the convergence curve of strain exhibited initial oscillations that stabilized with mesh refinement.

Figure 17: Graph representing strain for geometry with shim

The necessity to pick elements of high quality in areas of high strain gradients was one major outcome of the strain analysis. The presence of poorly formed elements in some parts can lead to unrealistic predictions of strain and numerical instability in such regions. To enhance accuracy, the research made sure that the elements in the areas of high strain had a low aspect ratio as well as low skewness.

3.5.5. Verification of Mesh Convergence

To confirm mathematically the convergence of the finite element solution, a percent error analysis was carried out. The percent error was calculated by comparing the numerical solutions with different mesh sizes to the results of the finest mesh (the most refined solution). This analysis provided a quantitative measure of convergence, which assured that the selected mesh size provided adequately accurate results.

The percentage error of deformation reduced notably as the mesh was refined, with the readings going below 1% at the last level of refinement. This observation corroborated the fact that the results of deformation had attained a stable and correct solution. The values of stress and strain initially had higher percentage errors at the beginning levels of mesh refinement; however, the errors progressively decreased as the mesh was further refined to the level of convergence stabilization.

Among the significant observations was that stress and strain required a finer refinement of the mesh to converge than deformation. This agrees with classical FEA concepts in which stress and strain fields are more susceptible to mesh density since they are based on derivatives of displacement.

3.5.6 Computational Efficiency and Practical Considerations

Mesh refinement was the cause of higher accuracy but at the same time also brought about a large rise in computational time and memory demands. Computational cost grew tremendously

as finer meshes were employed because of the larger number of elements and degrees of freedom within the system. It was a situation that demanded a balance between accuracy and efficiency, and the selected mesh delivered sufficient accuracy without exorbitant computational cost. Figures 18 and 19 show the mesh selected after the mesh convergence study for both geometries.

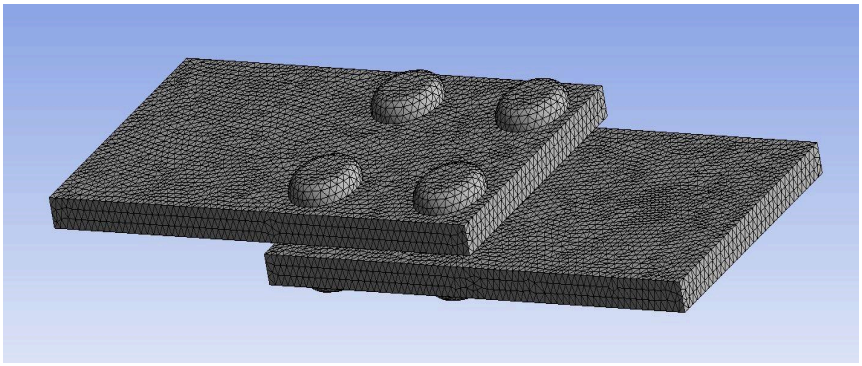

Figure 18- Selected mesh for geometry without shim

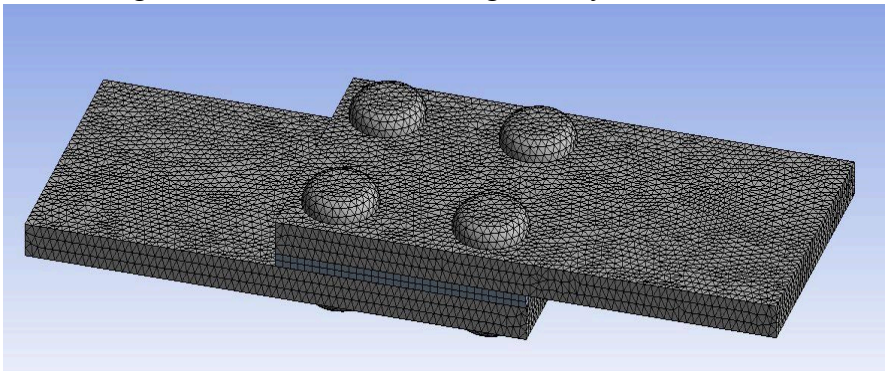

Figure 19- Selected mesh for geometry with shim

IV. Computational Analysis for Deformation, Stress, and Strain.

The analysis showed that a mesh with an element size of 0.0015 m was determined to be the most favorable arrangement for the final analysis. The chosen mesh size provided a proper trade-off between accuracy and computational cost, ensuring in this way that the results were reliable without causing unnecessary computational effort.

4.1 Analysis of Geometry without a Shim.

4.1.1 Deformation

Mesh convergence test determined that the ideal mesh C of 0.0015 m is most suitable for the finite element analysis (FEA). The following section gives a comprehensive analysis of deformation, stress, and strain of both geometries. The aim is to analyze the two cases from the perspective of determining the effect of the shim on structural stability, load carrying capacity, and performance.

Table 11: Results of deformation of geometry without shim

Without Shim	Minimum (mm)	Maximum (mm)	Average (mm)
Deformation	0	11.496	4.6299

The deformation analysis provides important data regarding the displacement of the structure under the applied external loads. When no shim is used, the maximum deformation occurs in the regions that are farthest from the fixed support, especially in the vicinity of the load points. The phenomenon follows expectation as these regions experience maximum bending moments and are more prone to displacement. The absence of additional reinforcement provides greater flexibility in the system, leading to increased deformation under the same loading conditions.

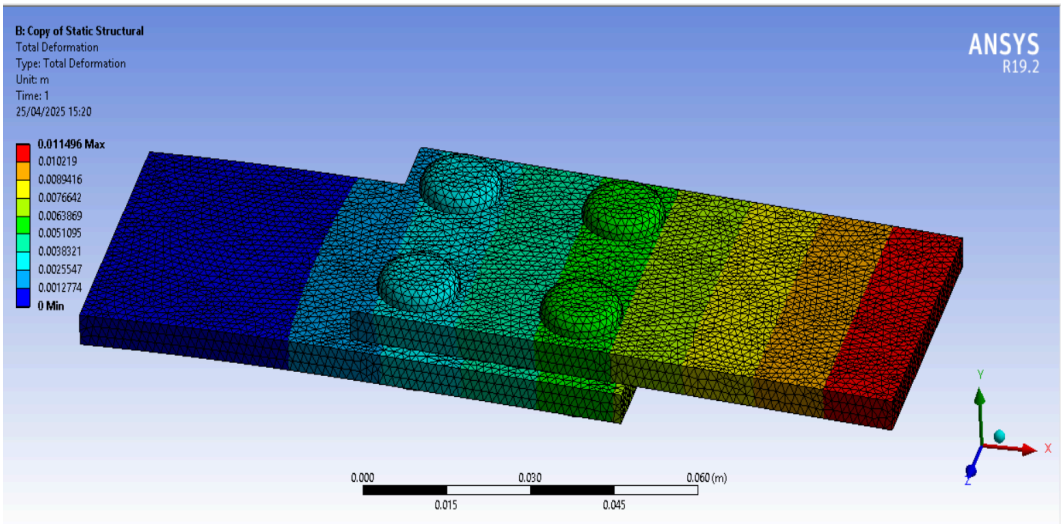

Figure 20- Deformation contour of geometry without shim.

Also, the absence of additional system stiffness causes localized regions to have characteristically more displacement than the adjacent areas. The uneven deformation is an indication that portions of the structure may undergo considerable deflection, which may affect performance and structural safety. The deformation pattern observed reflects a smooth

changeover from the shimmed area to the unrestrained boundaries, which indicates that the numerical model performs well and doesn't show any computational abnormalities. However, the overall level of deformation suggests that without the presence of a shim, the structure can experience displacements that go beyond tolerable limits, causing operational inefficiencies or increased exposure to structural collapse in the long run.

4.1.2 Stress

Stress analysis is of the utmost importance in comprehending the internal distribution of forces in the structure. Without a shim, the stress distribution is extremely non-uniform, with peak stress concentrations located in the region of the points of load application and abrupt changes in geometry. Such areas of high stress are significant in that they may be points of failure in case of long-term loading or cyclic stress oscillations within the material.

Table 12: Results of the stress of geometry without a shim

Without Shim	Minimum (MPa)	Maximum (MPa)	Average (MPa)
Stress	0.038235	426.65	61.629

Furthermore, the values of the von Mises stress in some areas are beyond the allowable stress limits of the material, showing that the structure is susceptible to failure when subjected to sustained or high loads. The stress distribution patterns show that zones with sudden changes in geometry, i.e., corners and edges, have higher stresses than those with smoother surfaces. The high stress gradient indicates that the structure is exposed to a non-uniform distribution of stress, which can cause local failure or premature fatigue of the material.

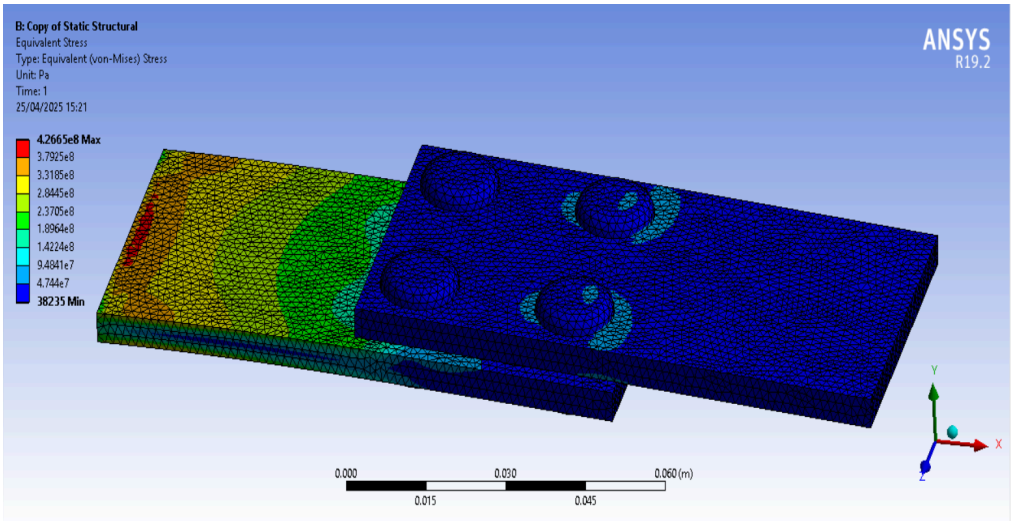

Figure 21 - Stress contour of geometry without shim.

In general, the study shows that the component, without a shim, has poor reinforcement in certain critical areas with ensuing greater concentrations of stress, which can make structural realignment necessary to increase durability and safety.

4.1.3 Strain

Strain analysis complements the results obtained from stress analysis by highlighting areas where the material is subjected to significant elongation or compression. Without a shim, the strain measurements are higher in areas that are subjected to bending and local stresses. The areas showing the highest strain correspond well to the regions of high stress, thus confirming that these locations have the highest material deformation under load.

Table 13: Results of the strain of geometry without a shim

Without Shim	Minimum (με)	Maximum (με)	Average (με)
Strain	0.53853	6022.2	912.38

The other noteworthy observation is the localized concentration of strain in certain regions, meaning that elongation of the material is not evenly distributed. The phenomenon presents a potential risk of surpassing the elastic limit of the material, thereby resulting in plastic deformation or damaging the structure in the long term. Thinner sections of the structure, specifically, undergo higher strain because of the lack of extra support, thereby elevating the risk of failure.

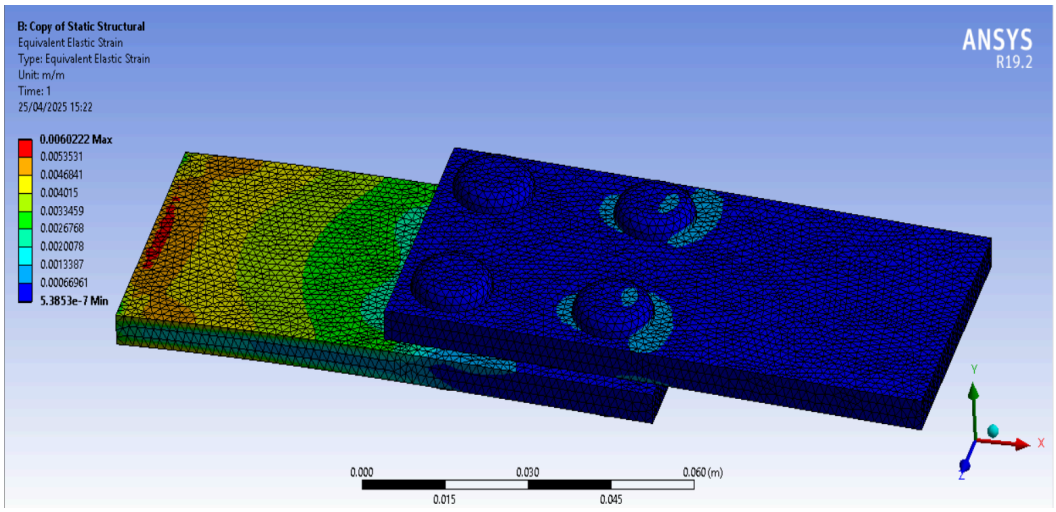

Figure 22 - Strain contour of geometry without shim.

The results show that, without a shim, the structure becomes more prone to serious deformation, stress accumulation, and potential failure, all of which can weaken its mechanical integrity over time.

4.2 Analysis of Geometry with a Shim.

4.2.1 Deformation.

The utilization of a shim tremendously changes the structural behavior by adding support and stiffness, consequently decreasing overall deformation. The findings indicate that maximum deformation readings are considerably reduced compared to instances where no shim is utilized. Having the shim enables the applied load to be more evenly distributed, such that no specific region is under an excessive displacement.

Table 14: Results of deformation of geometry with shim

With Shim	Minimum (mm)	Maximum (mm)	Average (mm)
Deformation	0	10.642	4.3541

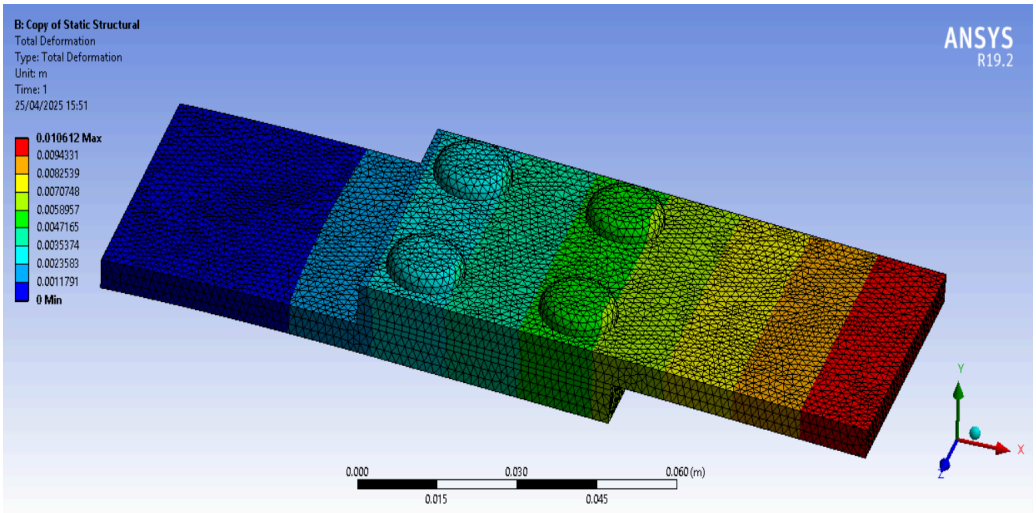

Figure 23- Deformation contour of geometry with shim.

Moreover, with the shim inserted, the structure has greater rigidity, thereby limiting excessive deflection. The deformation pattern remains even, confirming the assertion that the load-carrying capacity of the structure has been enhanced. The decrease in displacement confirms that the structure is able to bear higher loads without losing shape and functionality, hence enhancing overall performance. Including the shim also produces a more uniform transfer of load, reducing the likelihood of localized weaknesses that could lead to the structure becoming unstable.

4.2.2 Stress

The stress analysis for the situation with a shim shows a noticeable reduction in the maximum stress levels compared to the previous case. The shim works to transfer the load over an extended surface area, thus reducing the intensity of localized stress concentrations. The design in this way averts any specific area from withstanding extremely high stresses, which can lead to material fatigue or failure.

Table 15: Results of the stress of geometry with the shim

With Shim	Minimum (MPa)	Maximum (MPa)	Average (MPa)
Stress	0.049335	413.48	42.246

In this case, the von Mises stress values are within acceptable material limits, which implies that the structure is functioning in the safe region. The stress distribution patterns exhibit a smoother stress transition among various areas, proving that the introduction of the shim decreases abrupt stress gradients. By reducing such stress variations, the likelihood of stress-related failures, like cracking or yielding, is greatly diminished.

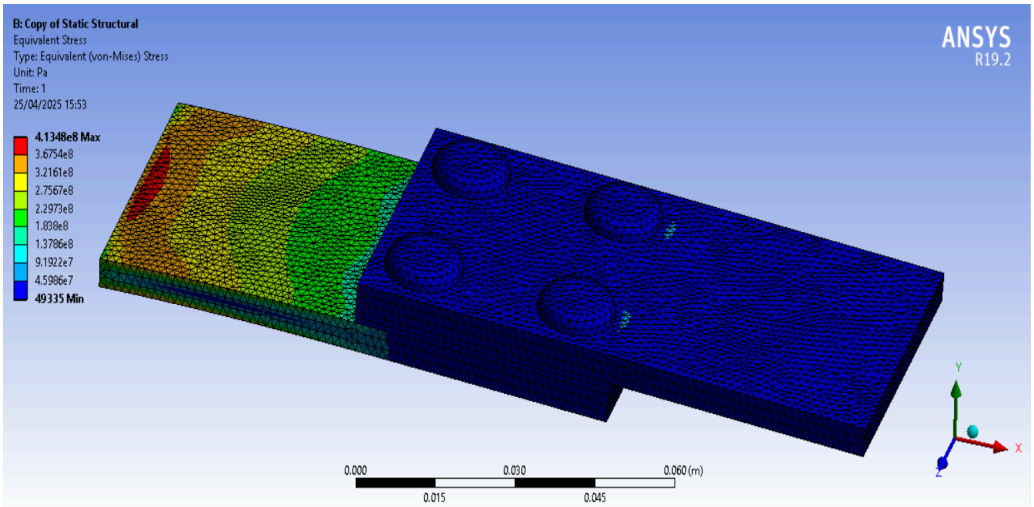

Figure 24- Stress contour of geometry with shim

The above argument reinforces the idea that the presence of a shim is paramount in increasing the structural strength of the component and minimizing the risk of mechanical failure when subjected to working loads.

4.2.3 Strain

The strain distribution for the case with a shim shows a considerable improvement in structural effectiveness. The levels of measured strain are much lower in comparison with the no-shim case, which means that there is less elongation of the material under the same loading conditions. This strain reduction makes the structure stronger in resisting forces from the outside and holding its original shape.

Table 16: Results of the strain of geometry with the shim

With Shim	Minimum (με)	Maximum (με)	Average (με)
Strain	2.5057	13296	681.85

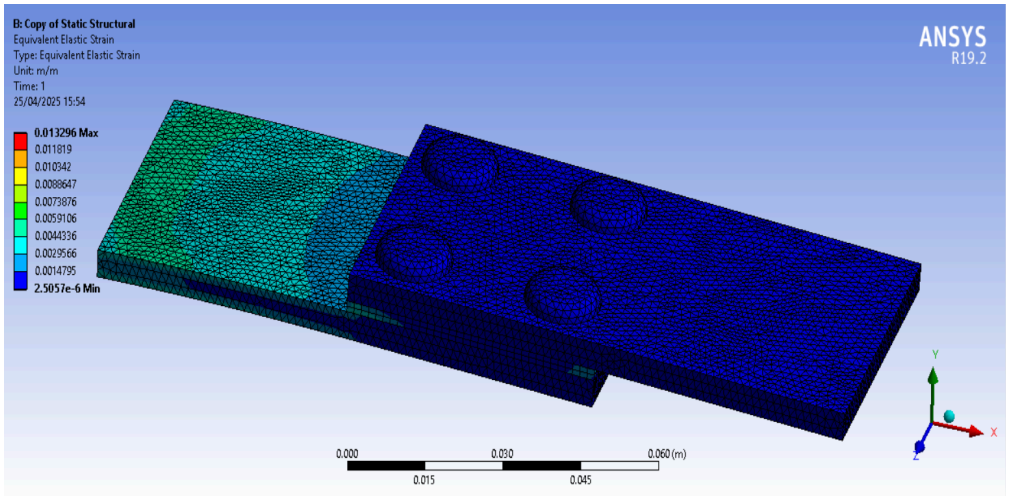

Figure 25- Strain contour of the geometry with the shim

The results indicate that strain distribution is relatively evenly distributed throughout the structure, indicating that there is no region that deforms excessively. This condition ensures that the material is well within its elastic limits, thus eliminating the possibility of permanent deformation. Additionally, the inclusion of the shim provides strength to key points, hence reducing localized strain concentrations that are likely to result in long-term structural degradation.

The detailed strain analysis corroborates that the shim greatly enhances the longevity of the component, minimizes the likelihood of failure, and enhances the overall structural stability under loads.

4.3 Comparative Analysis.

The results from both cases highlight the crucial role that the shim plays in improving structural performance.

- In the case when there is no shim, the structure has higher deformation, higher stress concentrations, and higher strain values, which all point toward an increased probability of failure. The load distribution is not ideal, leading to unnecessary elongation of the material and buildup of stress in certain regions.
- The application of the shim results in a remarkable enhancement of the structural stress, strain, and deformation responses. The distribution of loads is made more uniform, the maximum levels of stress are reduced, and the material receives decreased elongation, hence supporting an extended working life.

Table 17: Comparative analysis of geometries with and without shim

Parameter	Without Shim	With Shim
Deformation	Higher, localized in weak regions	Lower, more evenly distributed
Stress	High, with sharp gradients	Lower, more uniformly distributed
Strain	Significant, with risk of material failure	Reduced, ensuring material stability
Structural Integrity	Less stable, prone to excessive bending and stress	More stable, improved load distribution

V. Fatigue Analysis Techniques in FEM and ANSYS

Fatigue analysis is an important consideration of finite element analysis when determining durable components that have been subjected to cyclic loads. ANSYS provides different methods to perform fatigue analysis; some use empirical equations while others use numerical methods to estimate the fatigue life and crack growth. Insight into the mechanics of these equations will help the engineer in interpreting results and thus designing components that can last longer. Generally, ANSYS uses the Stress-life (S-N) Method, the Strain-life (ε-N) Method, and fracture mechanics for crack growth analysis.

5.1 Stress-Life (S-N) Method

The stress-life (S-N) approach is used exclusively in high-cycle fatigue situations, where the material will experience elastic deformation over the duration of loading cycles. The S-N approach is based on experimental data which relates the stress amplitude applied to a specimen and the number of cycles to failure. The result is known as an S–N curve or Wöhler curve, a graphical representation of its fatigue behavior. A typical S–N curve is presented in Figure 26, highlighting sections for low-cycle fatigue (LCF) and high-cycle fatigue (HCF). In the LCF section, the material will experience plastic deformation, and will fail in fewer cycles by producing a higher stress amplitude, whereas the HCF section has longer life under lower stress amplitudes, resulting in a largely elastic response from the material. Thus, this figure is integral to understanding fatigue analysis, while visually separating sections for each regime for an evaluation of structural fatigue in an aerospace application.

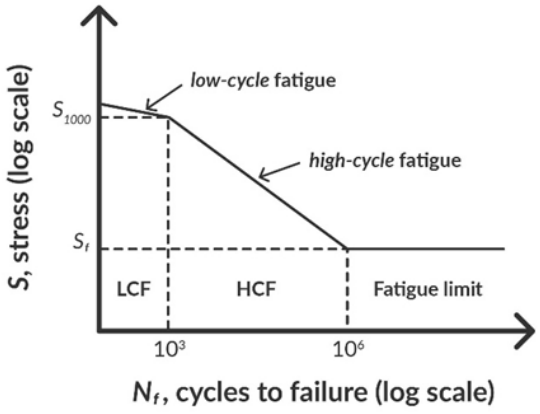

Figure 26 -Example of a S-N curve
[34]

In practice, the high-cycle fatigue region of the S-N curve can be represented mathematically using Basquin's equation, which relates the stress amplitude to the number of reversals to failure. ANSYS implements this formulation for fatigue life prediction under elastic conditions as:

$$\sigma_\alpha = \sigma_f' (2N_f)^b \quad (6.1)$$

Where σ_α represents the stress amplitude, σ_f' is the fatigue strength coefficient, N_f is the number of cycles to failure, and b is the fatigue strength exponent. These values are derived from material properties and experimental data.

To consider the mean stress effects from fatigue analysis, ANSYS has various correction models available – Goodman, Gerber, and Soderberg. The Goodman relation adjusts the allowable fatigue stress when there is a non-zero mean stress and the fatigue strength decreases as mean stress increases.

$$\frac{\sigma_a}{\sigma_f} + \frac{\sigma_m}{\sigma_u} = 1 \quad (6.2)$$

Where σ_m is the mean stress, σ_f is the fatigue strength at a given life, and σ_u is the ultimate tensile strength.

The Gerber model has improved accuracy over the Goodman relationship, primarily because the Gerber model assumes a parabolic relationship between the mean stress and alternating stress. This assumption makes the Gerber model particularly useful for predicting the fatigue life of components that will undergo moderate to high plastic deformation. Still, the Gerber model is empirical in nature and could lack conservativeness in other critical applications. In contrast, the Soderberg criterion is prevalent because it has a larger measure of conservativeness. It's use of the yield strength in place of the ultimate tensile strength that Goodman and Gerber models used circumvents a more conservative limit for the fatigue stress that can be utilized. Especially when dealing with critical aerospace components, the need to prevent failure is paramount even when considering the worst-case loading as a fatigue loading. The Soderberg line is not an exact line because it is linear; however, it can be used purely as a preliminary design sketch point that defines appropriate limits of fatigue strength where there is uncertainty in loading or material behavior.

Although the models described above are fitted for constant amplitude loading, a great number of real-world applications will involve a variable amplitude fatigue scenario with cumulative damage effects. The Goodman and Gerber models replaced ultimate tensile strength with yield strength, so the Soderberg relationship provides an even more limiting bound on assumed allowable fatigue stress. This is especially important for safety-critical aerospace applications, whereby failure under the worst-case loading must be avoided. As the Soderberg line is the straight-line approximation of the Goodman and Gerber models, they are often used in preliminary design phases or in situations where significant uncertainty exists surrounding loading or material response.

However, if the variable amplitude loading on a given component causes uneven damage due to fatigue, then ANSYS assumes Palmgren-Miner's Rule as a one-dimensional, linear damage accumulation approach. When the cumulative damage reaches a certain value, failure occurs:

$$D = \Sigma \frac{n_i}{N_i} \quad (6.3)$$

Where n_i represents the number of applied cycles at a given stress level, and N_i is the corresponding fatigue life at that stress level. When the summation of fatigue damage reaches 1, the material is predicted to fail.

5.1.1 Advantages:

1) Simplicity and Efficiency:

The procedure is quite simple and computationally efficient, which makes it a perfect candidate for a preliminary design concept analysis. It requires a small number of parameters, and the main input for them is the S-N curves from standardized tests.

2) Well Established Data:

Large amounts of experimental data on many materials exist in engineering handbooks, thereby limiting the number of complicated tests that have to be performed for specific materials.

3) Ideal for High Cycle Fatigue Conditions:

Most effective in determining fatigue life in components subjected to cyclic loads in which stress levels do not exceed the yield strength.

5.1.2 Disadvantages:

1) Limited Applicability in Low Cycle Ftigue Conditions:

The S-N method proves ineffective in situations of low-cycle fatigue (LCF), during which plastic deformation is characterized as significant.

2) Mean Stress Effects Require Corrections:

Since the majority of the S-N curves were obtained under fully reversed loading conditions (R=-1), adjustments such as the Goodman, Gerber, or Soderberg correction models would be necessary in the presence of mean stresses.

3) Environmental and Surface Overlooked:

The method does not inherently take into account factors such as surface roughness, temperature variations, or corrosive environments, all of which would heavily influence the fatigue life.

5.1.3 Limitations:

1) Lacks Crack Initiation Insight:

With the S-N method, fatigue failure is predicted without modeling the crack initiation and propagation stages. It is less efficient for defect-sensitive materials or notched components, in which local plastic deformation is possible.

5.2 Strain-Life (ε-N) Method

Low-cycle fatigue, in any given case, prevails when the Strain-Life approach is applied. This method does, however, take plastic deformation into account, as opposed to the Stress-Life analysis, which relies purely on elastic behavior. This indicates its critical importance in predicting the failure of any component that has to sustain high stresses and strains.

Fatigue life in this regime is governed through the Coffin-Manson equation, which is based on the contribution of both elastic and plastic strains.

$$\varepsilon_a = \frac{\sigma_f'}{E}(2n_f)^b + \varepsilon f'(2N_f)^c \quad (6.4)$$

Where, ε_a is the strain amplitude σ_f' is the fatigue strength coefficient, E Young's modulus N_f is the number of cycles to failure, and b the fatigue strength exponent. The second term introduces ε_f', which is the fatigue ductility coefficient and the fatigue ductility exponent, to capture the effects of plastic deformation.

To improve the accuracy of estimating fatigue life under mean stress conditions, ANSYS implements mean stress correction models in the strain-life approach. The mean stress correction can be included in one of two ways: Morrow's method and the Smith-Watson-Topper (SWT) method. The Morrow method modifies the elastic portion of the strain-life equation by subtracting the mean stress from the fatigue strength coefficient. This modification results in a more accurate estimate of fatigue life in cases of tensile mean stresses, particularly in regimes of high-cycle fatigue where elastic strains dominate.

The modified strain-life equation incorporating Morrow's correction is given as:

$$\sigma_{fcorr}' = \sigma_f' - \sigma_m \quad (6.5)$$

In contrast, the Smith-Watson-Topper approach allows for consideration of both the straining maximum stress and the amplitude of variabilities in strains.

$$max(\sigma_{max} \cdot \varepsilon_a) = constant \quad (6.6)$$

These corrections serve as improvements for damage-prone fatigue life predicted at every material undergoing plastic straining.

5.2.1 Advantages:

1) Accurate for LCF conditions:

The ε-N method considers both elastic and plastic strains, ensuring correct values and predictions for components at high stress with local plastic deformation.

2) Captures Crack Initiation:

The ε-N approach, unlike the S-N method, models the initiation of the crack, giving insight into the early stages of the fatigue damage process.

3) Material Behavior in Plastic Deformation:

The combination of elastic strain components with the Coffin-Manson equation allowed for accurate predictions of fatigue behavior for materials undergoing cyclic hardening or softening.

4) Mean Stress Corrections Integrated:

Methods such as Morrow's correction and Smith-Watson-Topper (SWT) increase their accuracy under mean stress conditions.

5.2.2 Disadvantages:

1) Complex and Computationally Intensive:

The strain-life method requires comprehensive, detailed material properties like fatigue strength coefficient and fatigue ductility coefficient, some of which may be scarce for some materials.

2) Material Testing required:

Accurate ε-N curves demand specialized testing, thereby escalating time and cost in material characterization.

3) Less reliable in HCF Conditions:

The ε-N method is of limited applicability for predicting fatigue life in conventionally treated materials with insignificant plastic strains, such as high-strength steels under conditions of low stress.

5.2.3 Limitations:

1) Limited Crack Propagation Prediction: The ε-N method gives attention to crack initiation only and not detailed crack growth modeling. For components where crack propagation is the key mechanism of failure, features of fracture mechanics would be warranted.

5.3 Fracture Mechanics Approach (Crack Growth Analysis)

Once a crack has formed on its own, fracture mechanics methods come into play to predict further growth of the crack, using cyclic loading. Such a situation is highly applicable in damage-tolerant designs, as every engineer wishes to provide themselves with the sort of information that makes it possible to assess how long a crack can further develop before producing an effect characterized as catastrophic. Crack growth rates are defined in terms given by Paris' Law, employed by ANSYS.

$$\frac{da}{dN} = C(\Delta K)^m \qquad (6.7)$$

Where $\frac{da}{dN}$ represents the crack growth rate per cycle, ΔK is the stress intensity factor range, and C and m are material-specific constants. By integrating this equation, ANSYS determines the number of cycles required for a crack to grow from an initial size to a critical size.

In more advanced fatigue crack growth predictions, ANSYS supports other modeling frameworks, such as those by NASGRO and Walker equations, in refining estimates by considering load ratios and loading conditions specific to a certain material.

5.3.1 Advantages:

1) Accurate Crack Growth Prediction:

The principle outlines the fracture mechanics method of growth as Paris' Law, which is utilized to find defects in critical structures effectively.

2) Applicable for Defect-Sensitive Materials:

Certain fracture mechanics are rated very high in incidences of rapid development of sudden cracks, precisely in the case of aerospace alloys or welded structures.

3) Ideal for Predicting Residual Life:

By estimating the number of cycles taken for a crack to extend till it has reached a borderline, engineers can predict its remaining life and thus plan the subsequent checks.

5.3.2 Disadvantages:

1) Requires detailed crack information:

For a precise prediction, the initial crack size and geometry, along with stress intensity factors, must be measured carefully, which is quite difficult at times.

2) Computational Complexity:

Simulating crack growth involves a high computational load, especially under non-linear conditions or under multi-axial stress states.

3) Material-specific Calibration Required:

The variables C and m in Paris' Law need extensive calibration through experiments for each material.

5.3.3 Limitations:

1) Poor at predicting Crack Initiation:

Irrespective of whether there is a flaw or crack present, fracture mechanics does not predict when or how cracks would occur. For cases wherein crack initiation is the dominant mode of failure, the best alternative is to apply the strain-life methodology.

5.4 Fatigue Analysis Implementation in ANSYS

A short introduction to the fatigue analysis tools available in ANSYS will follow next. The Workbench Fatigue Module presents basic fatigue analysis based on the S-N or S-N method or ε-N method. This includes advanced functionality incorporating rainflow counting, a method for extracting useful fatigue cycles from complex history paths, along with various methods for mean stress correction for improved life predictions.

Table 18: Comparison of fatigue methods.

Method	Best for	Advantages	Disadvantages	Limitations
Stress-life (S-N)	High-Cycle Fatigue	Simple, fast, widely available data	Poor for LCF requires mean stress corrections	Cannot predict crack initiation
Strain-life (Ɛ-N)	Low-Cycle Fatigue	Accurate for plastic deformation, models the crack initiation	Complex material data required, computationally intensive	Limited for HCF conditions
Fracture Mechanics	Crack Growth Prediction	Accurate for defect-prone materials, effective for residual life prediction	Requires crack size data, demanding computation	Does not predict crack initiation

Finally, ANSYS Paris Law for Crack Growth is utilized in a fracture mechanics-based fatigue analysis. It assists by giving engineers a forecasting tool for crack propagation and component failure due to fatigue per se.

5.5 Choice of Fatigue Assessment Techniques Guided by Structural Information

Fatigue analysis is critical to predicting the failure of components under cyclic loading conditions. Selection of the appropriate methodology is critical in making accurate life predictions and supporting component design to withstand operational loads. The following report compares different fatigue analysis methods on the basis of the provided values of deformation, stress, and strain for two designs: one with a shim and one without a shim.

5.5.1 Structural Data Overview

As discussed in the structural analysis, both the shimmed and non-shimmed aluminum alloy models were subjected to equivalent loading and boundary conditions to evaluate their mechanical behavior. The results are maximum, minimum, and average values for deformation, von Mises stress, and equivalent elastic strain. These values, discussed in Chapter 4, assist in choosing the proper method of fatigue analysis in this study.

Without Shim:

- Maximum deformation: 11.496 mm
- Maximum stress: 426.65 MPa
- Maximum strain: 6022.2 με

With Shim:

- Maximum deformation: 10.612 mm
- Maximum stress: 413.48 MPa
- Maximum strain: 13296 με

5.5.2 Methodological Choice for the Fatigue Analysis

Fatigue analysis methods can be broadly categorized into three main approaches: the Stress-Life (S-N), Strain-Life (ε-N), and Fracture Mechanics approaches. The choice of method depends on parameters like stress levels, strain characteristics, and the expected number of cycles to failure.

5.5.2.1 Stress-Life (S-N) Approach

The S–N method is applicable to HCF conditions in which the material is sufficiently elastic and the stress amplitudes are at low levels, or during HCF with the HCF maximum stress, given the study's data. The maximum stress values, 4.2665×10^{8} Pa for the non-shimmed, and 4.1348×10^{8} Pa for the shimmed geometry, demonstrated that the material has remained below the typical yield strength of the aluminum alloy of which it is made, so is still in the HCF regime for the S−N method. However, raw stress values are not enough to characterize the fatigue response, in particular when localized plastic strain is evident. Therefore, while it is appropriate to apply the S−N method in purely elastic conditions, the evaluation of S−N must be reconsidered based on these strain-based observations.

5.5.2.2 Strain-Life (ε-N) Methodology

The strain-life (ε-N) method is utilized to analyze fatigue behavior under plastic-response circumstances and is generally known as low-cycle fatigue (LCF) conditions. In this study, the structural model maximum strain values were 6.0222×10^{-3} (non-shimmed geometry) and 1.3296×10^{-2} (shimmed geometry). These strains are much larger than the elastic strain limit of roughly 0.002 (0.2%) generally seen for aluminum alloys. We can assess that both the non-shimmed and shimmed geometrics experience some degree of plastic strain. Again considering the effects of plastic deformation, the ε-N method has the least complex and most applicable conditions to predict fatigue life by examining the effects of elastic strain and plastic strain under cyclic loads.

5.5.2.3 Fracture Mechanics Approach

This method is utilized in environments where existing cracks pose difficult challenges, thus enabling the evaluation of crack propagation rates and predicted failure times. Since the information presented does not have specific details about the cracks, this method is not the most appropriate for this evaluation.

5.5.2.4 Suggested Methodological Framework for Investigation

The strain-life method was selected instead of the stress-life method because the strain-life method is a better framework for analysing components that typically undergo localized plastic deformation. The stress-life method is more common for high-cycle fatigue under purely elastic conditions, particularly for fatigue evaluation of components that typically remain elastic. However, the strain-life method provides a better representation of fatigue behaviour when material experience both elastic and plastic strain. Regarding the loading type and material behaviour observed in this study, the strain-life method was the more suitable framework for evaluating fatigue performance.

VI. Strain-Life Analysis.

This chapter describes the strain-life fatigue evaluations performed on both shimmed and no shim geometries. The approach to the evaluation utilizes strain-life (ε–N) method of fatigue analysis because it can better model the fatigue response in an area where the material experiences plastic strain. The body of the chapter describes the material data, implementation of the Morrow mean stress correction method and the evaluation parameters of fatigue life, damage and safety factor.

6.1 Engineering data and Fatigue Analysis Setup.

Engineering data for the strain-life fatigue analysis was defined individually for the two materials used in this study: aluminum alloy for both geometries, and epoxy resin specifically for the shimmed configuration.

The material properties for the aluminum alloy were obtained from MMPDS-13, which is recognized as a database on aerospace materials and included Young's modulus, Poisson's ratio, yield strength and ultimate tensile strength. For strain-life fatigue evaluation, the fatigue parameters of aluminum, such as the fatigue strength coefficient, fatigue ductility coefficient, and their respective exponents, were adopted from literature sources [35][36]. The properties for epoxy resin were obtained from composite material handbooks and fatigue research on polymer-based shims.

The Morrow mean-stress-correction procedure was chosen for use in the fatigue analysis to account for the action of non-zero mean-stress, which is significant when analyzing load cases with effects from pressurization and considering multiaxial loading and loading paths. Three output parameters were analyzed: fatigue life (the estimated number of cycles a material can withstand in the defined load conditions), fatigue damage (the measure of how much of total fatigue life has been used after the defined cycles have been imposed), and safety factor (the measure of how close the structure is to fatigue failure) with consideration to that when safety factor values fall below one, those are regions of concern.

For consistent and meaningful comparison, the same loading conditions were applied to both geometries. A total of 50,000 load cycles was chosen for the fatigue simulation for each configuration. This value is consistent with previous fatigue literature for aluminum alloy components in the low-cycle fatigue (LCF) regime, where plastic deformation is substantial in affecting the fatigue life. Defining 50,000 cycles assures meaningful accumulation of fatigue damage in the fatigue analysis while remaining feasible for strain-life based evaluations of aerospace structures [37][38].

The load magnitudes, loading type, and boundary conditions were constant to both geometries in order to isolate the epoxy resin shim and ensure any differences in fatigue life, stress distributions or damage evolution could be assigned that the shim's presence or absence. The following sections discuss fatigue analysis results of both configurations and describe their fatigue response under cyclic loading in aerospace service conditions.

6.2 Analysis of Geometry without Shim

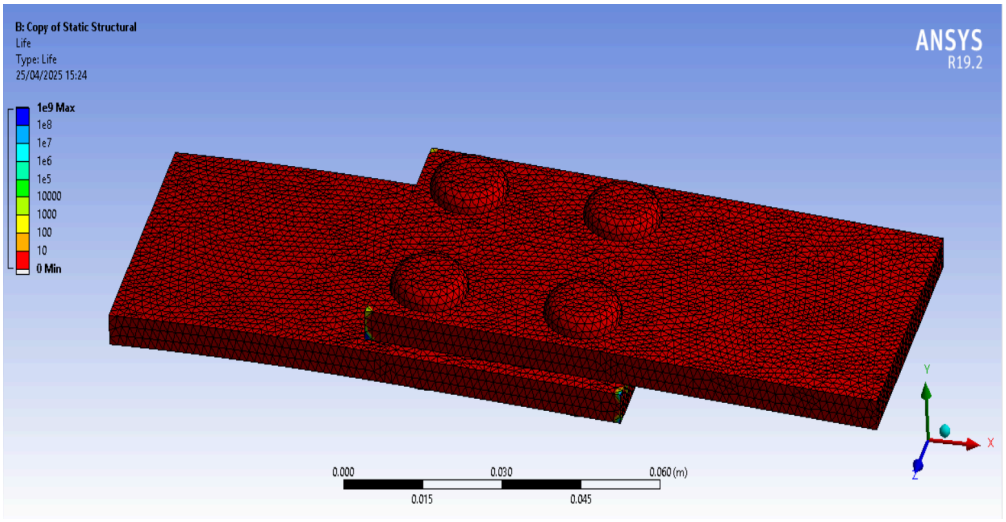

Figure 27- Fatigue life contour of the geometry without the shim

Table 19: Results of fatigue life of geometry without shim

Without Shim	Minimum	Maximum	Average
Fatigue life	0	1×10^9	2.207×10^5

Using the strain-life (ε–N) approach including the Morrow mean stress correction, the fatigue behavior of the non-shimmed aluminum alloy geometry was determined to represent a structurally undesirable fatigue behavior given the applied loading conditions. Low-cycle fatigue endurance was indicated across much of the geometry, as evidenced in Figure 27 with the fatigue life contour showing large areas of low cycle fatigue endurance, and a large area of critically low fatigue life across the component. The fatigue life contour is dominated by areas coded red indicating the early onset of fatigue failure across the component. The fatigue critical areas are concentrated approximately where the fixed boundary and load application regions are located, these regions are also where high stress concentrations were determined from the structural analysis.

Table 19 shows the numerical results associated to the fatigue life contour. The reported minimum fatigue life is 0 cycles. This means that the specified failure occurred immediately in certain localized areas, likely because of geometric discontinuities and stress risers. The maximum life reported was 1 x 10^9 cycles but this was only in the least load bearing areas Agian the average fatigue life reported of 2.21 x 10^5 cycles is a number far less than the expected design life of components subjected to service and failure from fatigue. Therefore it was clear that the design, and in its unshimmed state was very sensitive to degradation from fatigue after service. The results confirm the limitations of a component from solely utilizing aluminum alloy where no stress relieving interfaces are established and confirms the need to modify to evaluate

another configuration like the introduction of shimmed epoxy resin underneath the face pot to improve fatigue behavior.

Table 20: Results of fatigue damage of geometry without shim

Without Shim	Minimum	Maximum	Average
Fatigue Damage	5×10^{-5}	1×10^{32}	9.9777×10^{31}

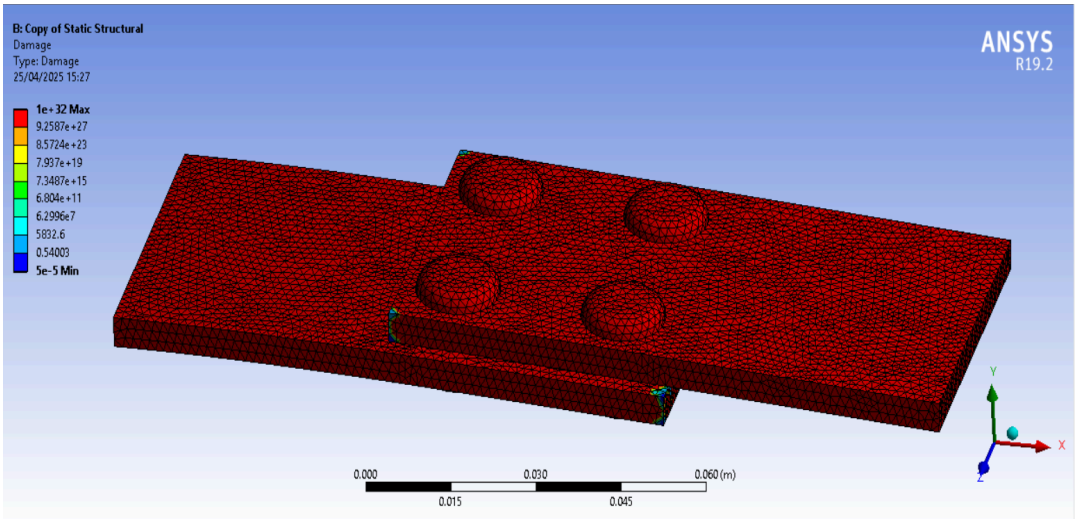

Figure 28- Fatigue damage contour of the geometry without the shim

The fatigue damage distribution for the model without shim geometry is provided in Figure 28. The contour plot provides a two-dimensional visualization of the accumulated fatigue damage from 50,000 load cycles. The non-dimensional modelling had higher damage levels towards the edge and near the load application area which were determined to be the areas of major stress concentrations previously and were reflected in those loads. The contour plot clearly shows that a significant area of the structure has moved into critical fatigue levels. The table below (Table 20) shows the minimum damage is 5.0×10^{-5}, the maximum is 1.0×10^{32} and the average is 9.9777×10^{31}. The damage values shown are not nominally normalized, but the exponential nature of the damage results, reinforces that significant corrosion had occurred over a the entire length of the component, further confirming the ineffectiveness of the non-shimmed application in cycling loads.

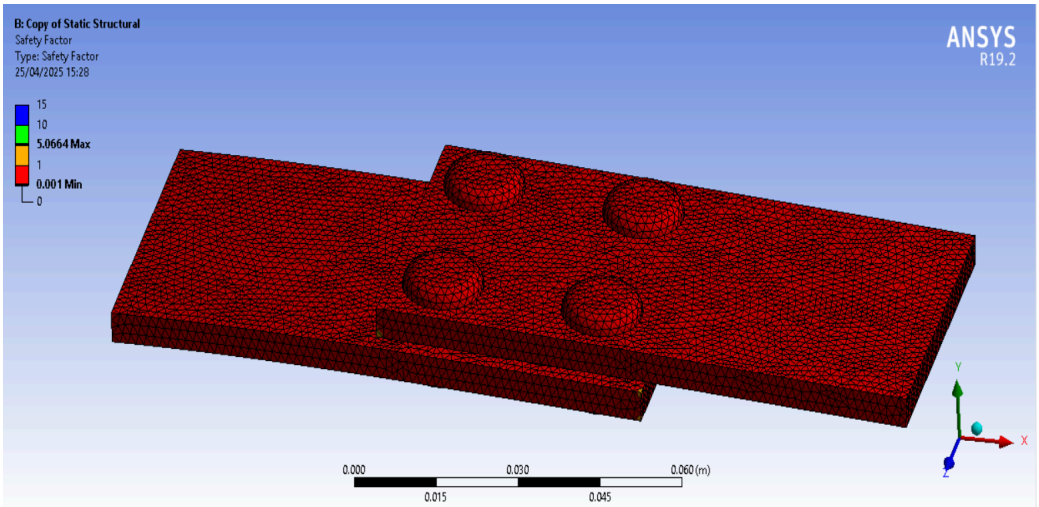

Figure 29- Fatigue safety factor contour of the geometry without the shim

Table 21: Results of fatigue safety factor of geometry without shim

Without Shim	Minimum	Maximum	Average
Fatigue Safety Factor	1×10^{-3}	5.0664	2.5127×10^{-2}

The high levels of accumulated damage at this early fatigue and load application stage highlight the structural inadequacies of the non-shimmed configuration under cyclic load. Figure 29 offers the fatigue safety factor contours for the same geometry. The contour is useful in identifying the amount of safety margin until fatigue failure occurs. The lower the safety factor, the greater the risk zone for fatigue failure. For most regions of the model, we can see from Figure 28 that safety factor contours are all well below 1.0, as would be expected especially near high-stress regions. This implies the non-shimmed condition does not possess adequate fatigue strength to endure cycles of loading. As noted in Table 21, with a minimum of 1.0 x 10-3, a maximum of 5.0664, and an average of 2.51 x 10-2. These results support the conclusion that much of the component operates below-stated safety limits and thus are highly prone to fatigue failure. Overall, fatigue life, damage, and safety factors confirm that the unshimming the aluminum alloy structural capability to endure cyclic loading is highly limited for aerospace applications.

6.3 Analysis of Geometry with Shim

The strain-life fatigue analysis of the shimmed geometry exhibited significantly better fatigue performance compared to the non-shimmed geometry. The average total fatigue life observed in figure 30, while subjected to cyclic loading, was a significant approx 5.1502×10^{7} cycles.

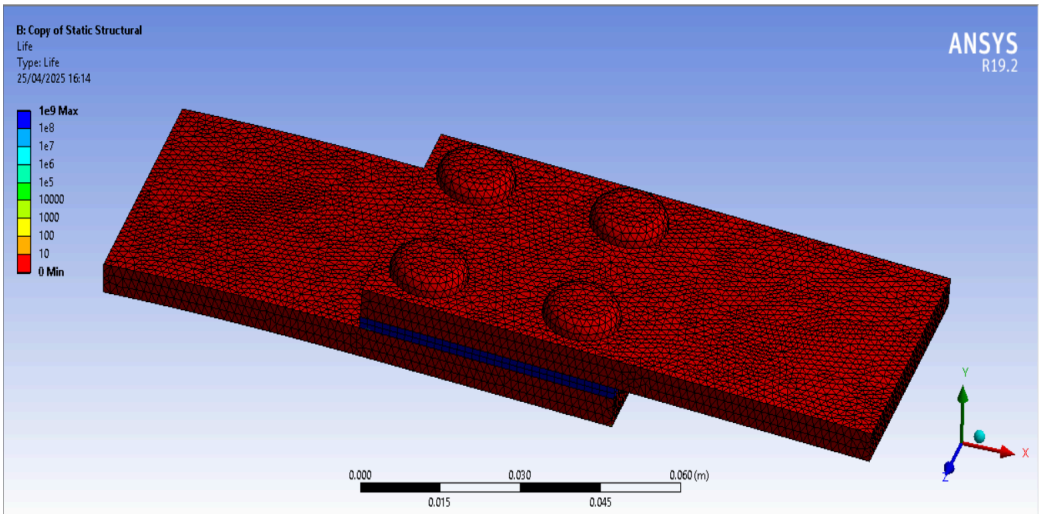

Figure 30- Fatigue life contour of the geometry with the shim

Table 22: Results of fatigue life of geometry with shim

With Shim	Minimum	Maximum	Average
Fatigue life	0	1×10^{9}	5.1502×10^{7}

The reason for the fatigue performance is attributed to the use of the epoxy shim, aiding in promoting and distributing stresses equally and lowered critical concentrators. This increases the fatigue life, and is even more prevalent at locations with high load transitions.

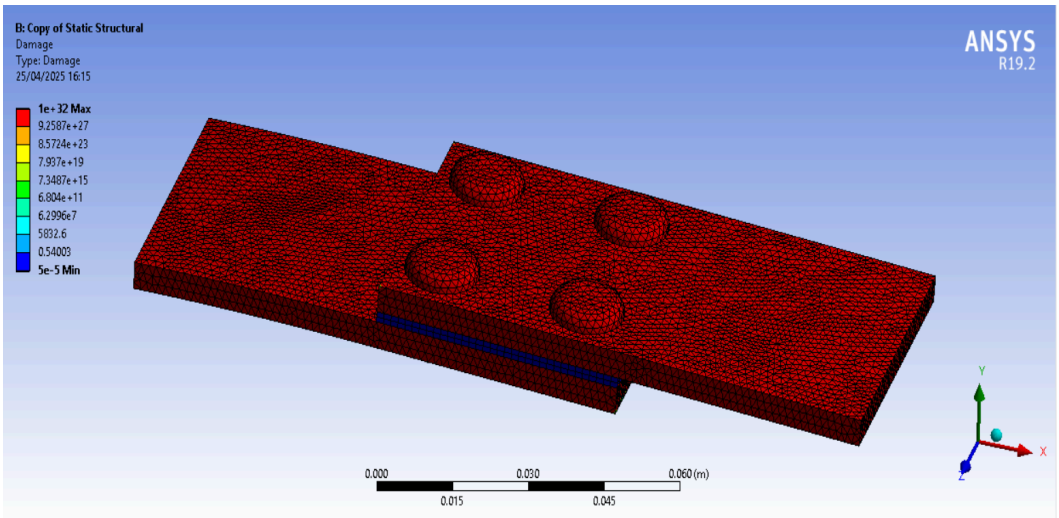

Figure 31- Fatigue damage contour of the geometry with the shim

Table 23: Results of fatigue damage of geometry with shim

With Shim	Minimum	Maximum	Average
Fatigue damage	5×10^{-5}	1×10^{32}	9.4471×10^{31}

The mitigation of where fatigue damage is distributed, figure 31 indicates that the shimmed geometry, has better fatigue life properties. Although there are discrete locations with damage values, the average damage value determined based on hypothesis testing, is less than that of the non-shimmed configuration, due to the structure only using a smaller fraction of its fatigue life, under the same number of loading cycles. Therefore, it means it was generally slower moving towards fatigue failure, and therefore were more serviceable in terms of sustained durability and scheduled maintenance.

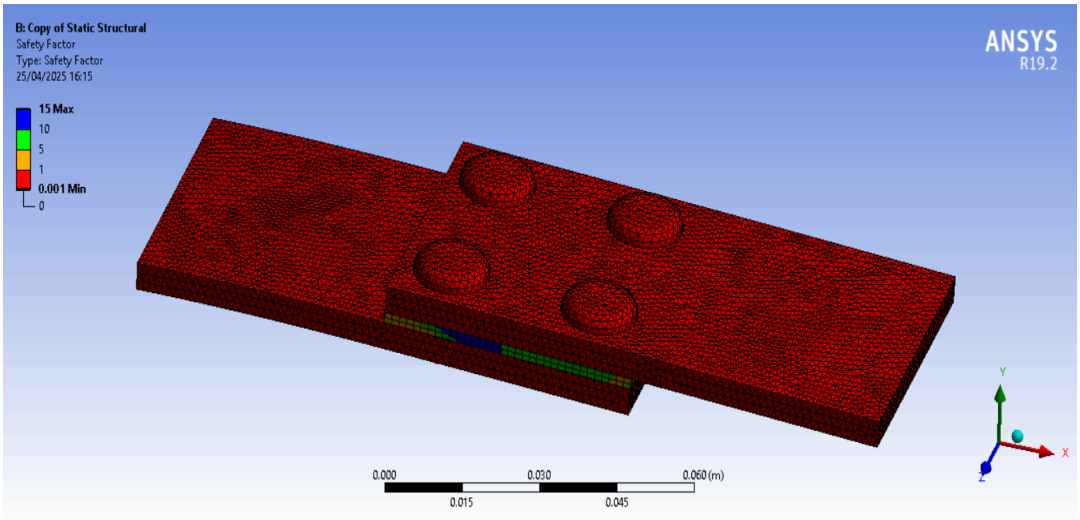

Figure 32- Fatigue safety factor contour of the geometry with the shim

Table 24: Results of fatigue safety factor of geometry with shim

With Shim	Minimum	Maximum	Average
Fatigue Safety Factor	1×10^{-3}	15	0.52275

In terms of safety factor, as in figure 32, the shimmed geometry had a higher number, an average of roughly 0.52, as compared to the non-shimmed geometry and indicates the component has a greater distance before fatigue failure, albeit still below the safety factor of 1.0 but which illustrates further that a shim is beneficial in a load sharing scenario.

Overall, the results indicate that shims are increasing their fatigue life, continue to aid reduce damage accumulation and continuing to improve the safety factor. There is a strong case, further support for using epoxy shims in fatigue critical aerospace applications generally, and particularly with composite thick-plate joints, to promote load uniformity for improving the reliability of the structure.

6.4 Comparative Discussion of Shimmed and Non-Shimmed Geometries

The comparison of the strain-life fatigue results from the shimmed and non-shimmed geometries clearly indicates that shimming is beneficial in the context of structural fatigue performance. The average fatigue life of the shimmed geometry was well more than two orders of magnitude higher than the average fatigue life from the non-shimmed configuration. The dramatic difference serves to highlight the ability of the shim to redistribute stress more uniformly and minimize the impact of peak strain zones that can be a big contributor to fatigue failure from those early cycles.

When gauging fatigue damage the items that had a shim, relative to the same geometry but without a shim, demonstrated less accumulation of damage from pre-continuous inspection loaded testing over the 50,000 interval. This further supports that the shimmed structure consumes less of its fatigue life compared to the identical components that were not shimmed, and also demonstrated that the shimmed item degraded at a much slower rate. These factors ultimately contributed to the shimmed assemblies representing more robust longevity under the same load and stress compared to assemblies subjected to fatigue-critical conditions.

The safety factors comparing the two configurations also show the improvement due to the shim. The safety factors were below the desired 1.0 safety factor level for both models. However, the shimmed model had a safety factor on average twenty times greater than the non-shimmed model. Hence, the shimmed structure would possess far more fatigue resistance and reliability than a non-shimmed structure. This is important for the aerospace industry where airframe safety and reliability are critically important.

The findings suggest that the epoxy shim does have a significant impact on the fatigue performance of structures while extending in service life under realistic loading scenarios. Therefore, the findings of this study provide a significant reason to include shimming practices for composite-metal joints (like those found in today's airframes) because of the criticality of longevity and fatigue resistance.

VII. Conclusion

This research successfully analyzed the role of shimming in the fatigue response of aluminium alloy structures using a strain-life fatigue analysis methodology. The static structural analysis investigated how the presence of a shim changed the deformation, stress, and strain responses of both models. The non-shimmed configuration reached higher maximum deformation and exhibited higher stress concentrations with thinner strain gradients, while also indicating a structural response that was more vulnerable under the specified loading conditions, and the shimmed configuration provided a relatively better stress distribution, although the local strain gradients were still large due to the presence of a shim, which is required for fatigue life.

In the fatigue analysis, with respect to the strain-life (ε–N) method with the Morrow mean stress correction, the results established a vast improvement in fatigue life and the safety margins of the shimmed model versus the non-shimmed model. The non-shimmed configuration had an averaged fatigue life that reached roughly 220,000 cycles and an average critical safety factor of 0.025. In contrast, the shimmed configuration had an averaged life of over 51 million cycles and a safety factor of roughly 0.52. Ultimately, the results distinctly demonstrate the ability of the shim to delay fatigue damage of the composite-metal hybrid structures while also enhancing the overall structural reliability when utilized as a shim.

The damage results underscored the benefits of the shimmed condition. Under a similar number of applied cycles, the shimmed component progressed through fatigue relatively slower and exhibited a more consistent damage distribution. The critical damage zones decreased and are entirely related to the durability and the service life of the components, relative to repeated loading as encountered in an aircraft.

The results are relevant to structural approaches for aircraft assemblies, such as the fuselage sections of the Boeing 787 Dreamliner, where composite fuselage sections utilize metal frames to connect sections, while shims to improve fit and load transfer. The results from this study validated the engineering reasons for shim use in fatigue components and assemblies in aerospace applications, and highlighted how shims can affect the performance and durability of advanced aircraft structures.

The data from the strain-life fatigue evaluation demonstrates clearly that employing an epoxy shim greatly improves the structural performance of composite-metal joints under cyclic loading conditions. The shimmed geometry showed longer fatigue life, less damage accumulation, and a much higher safety factor when compared to the non-shimmed shape. This increase in structural performance is predominantly due to the shim's ability to redistribute stress and strain more uniformly across the rivet joint preventing significant local stresses leading to the nucleation of fatigue cracks.

The results from employing the strain-life method with a Morrow mean stress correction provided a way to realistically represent the material behavior under the specified loads and counts. The fatigue analysis results (life, damage, and safety factor) revealed straightforward

measures of component reliability and showed that it was beneficial to add a shim for fatigue-critical joints.

These results support the engineering practice of using compliant shimming materials in multiaxial and cyclic loading applications, such as fuselage frame and stringer joints in aircraft, as in the Boeing 787. The presence of shims in these regions extends the service life of structural joints and safety margins.

Future studies should validate the simulations using actual experimental fatigue testing of actual specimens. Other studies may measure the effect of shim thickness, shim material, and loading spectrum to further enhance the fatigue performance of aerospace joints. In addition, thermal effects and environmental degradation of shim materials would improve future studies.

References

1. Davis, J.R., ed., Aluminum and Aluminum Alloys, ASM International, Materials Park, OH, 1993.
2. Hatch, J.E., Aluminum: Properties and Physical Metallurgy, ASM International, Materials Park, OH, 1984.
3. Suresh, S., Fatigue of Materials, 2nd ed., Cambridge University Press, Cambridge, UK, 1998.
4. Rioja, R.J., and Liu, J., "The Evolution of Al-Li Base Products for Aerospace and Space Applications," Metallurgical and Materials Transactions A, Vol. 43, No. 9, 2012, pp. 3325–3337. doi:10.1007/s11661-012-1155-z
5. Mishra, R.S., and Ma, Z.Y., "Friction Stir Welding and Processing," Materials Science and Engineering: R: Reports, Vol. 50, Nos. 1–2, 2005, pp. 1–78. doi:10.1016/j.mser.2005.07.001
6. Federal Aviation Administration, Metallic Materials Properties Development and Standardization (MMPDS-14), U.S. Department of Transportation, Washington, D.C., 2022.
7. Prasad, N.E., Wanhill, R.J.H., Aerospace Materials and Material Technologies, Volume 1: Aerospace Materials, Springer, Singapore, 2017. doi:10.1007/978-981-10-2134-3
8. Schijve, J., Fatigue of Structures and Materials, 2nd ed., Springer, Dordrecht, 2009. doi:10.1007/978-1-4020-6808-9
9. Pilkey, W.D., and Pilkey, D.F., Peterson's Stress Concentration Factors, 3rd ed., Wiley, Hoboken, NJ, 2008.
10. Laird, C., "The Influence of Metallurgical Structure on the Mechanism of Fatigue Crack Propagation," Fatigue Crack Propagation, ASTM STP 415, American Society for Testing and Materials, 1967, pp. 131–149.
11. Forman, R.G., and Mettu, S.R., "Behavior of Cracks in Structures Under Combined Loading and Corrosive Environments," NASA Technical Memorandum 104396, 1992.
12. Sutton, M.A., Orteu, J.-J., and Schreier, H.W., Image Correlation for Shape, Motion and Deformation Measurements, Springer, New York, 2009.
13. Peyre, P., et al., "Laser Shock Processing of Aluminum Alloys: Application to High Cycle Fatigue Behavior," Materials Science and Engineering: A, Vol. 210, Nos. 1–2, 1996, pp. 102–113. doi:10.1016/S0921-5093(96)10357-3
14. Hart-Smith, L.J., "Adhesive-Bonded Double-Lap Joints," NASA CR-112236, Langley Research Center, 1973.
15. Petrie, E.M., Handbook of Adhesives and Sealants, 2nd ed., McGraw-Hill, New York, 2007.

16. Xu, W., and Li, Q., “Finite Element Modeling of Epoxy-Based Shims in Bonded Aluminum Joints,” Journal of Adhesion, Vol. 93, No. 7, 2017, pp. 563–580. doi:10.1080/00218464.2016.1222574
17. Li, Y., et al., “Multifunctional Epoxy Composites Reinforced with Carbon Nanotubes for Structural Health Monitoring,” Composites Part B: Engineering, Vol. 176, 2019, Article 107307.
doi:10.1016/j.compositesb.2019.107307
18. Banea, M.D., and da Silva, L.F.M., “Adhesively Bonded Joints in Composite Materials: An Overview,” Proceedings of the Institution of Mechanical Engineers, Part L: Journal of Materials: Design and Applications, Vol. 223, No. 1, 2009, pp. 1–18. doi:10.1243/14644207JMDA219
19. Ferreira, J.A.M., Costa, J.D.M., and Reis, P.N.B., “Effect of Interfacial Compliance on Fatigue Performance of Bonded Aluminum Joints,” Journal of Adhesion Science and Technology, Vol. 25, No. 10, 2011, pp. 1313–1325.
doi:10.1163/016942411X567672
20. Petrie, E.M., Epoxy Adhesive Formulations, McGraw-Hill, New York, 2006.
21. Bagheri, R., and Marouf, B.T., “Fatigue and Fracture Resistance of Epoxy Nanocomposites,” Journal of Polymer Science Part B: Polymer Physics, Vol. 49, No. 9, 2011, pp. 539–554.
doi:10.1002/polb.22241
22. Kinloch, A.J., Adhesion and Adhesives: Science and Technology, Chapman and Hall, London, 1987.
23. Luo, Y., Liu, W., and Zhang, C., “Fatigue Crack Growth Behavior of Aluminum Alloy 2024-T3 under Different Stress Ratios,” *Materials*, Vol. 12, No. 2, 2019, pp. 1–14.
doi: 10.3390/ma12020271
24. Sadraey, M.H., *Aircraft Design: A Systems Engineering Approach*, John Wiley & Sons, Hoboken, NJ, 2012.
25. Federal Aviation Administration, “Aircraft Cabin Pressurization Control Systems,” Advisory Circular AC 25-20, U.S. Department of Transportation, Washington, D.C., 1996
26. Zienkiewicz, O. C., and Taylor, R. L., The Finite Element Method: Its Basis and Fundamentals, Butterworth-Heinemann, Oxford, UK, 2005.
27. Hughes, T. J. R., *The Finite Element Method: Linear Static and Dynamic Finite Element Analysis*, Dover Publications, New York, 2000.
28. Moaveni, S., *Finite Element Analysis: Theory and Application with ANSYS*, Pearson, Boston, 2014.
29. Belytschko, T., Liu, W. K., and Moran, B., *Nonlinear Finite Elements for Continua and Structures*, John Wiley & Sons, Hoboken, NJ, 2013.
30. Logan, D. L., *A First Course in the Finite Element Method*, Cengage Learning, Boston, 2011.

31. Rao, S. S., *The Finite Element Method in Engineering*, Butterworth-Heinemann, Oxford, UK, 2017.
32. Bathe, K. J., *Finite Element Procedures*, Prentice Hall, Upper Saddle River, NJ, 1996.
33. Fish, J., and Belytschko, T., *A First Course in Finite Elements*, John Wiley & Sons, Hoboken, NJ, 2007.
34. https://www.simscale.com/docs/simwiki/fea-finite-element-analysis/what-is-fatigue-analysis/, [accessed 2024].
35. Schijve, J., *Fatigue of Structures and Materials*, 2nd ed., Springer, Dordrecht, Netherlands, 2009.
36. Suresh, S., *Fatigue of Materials*, 2nd ed., Cambridge University Press, Cambridge, U.K., 1998.
    doi: 10.1017/CBO9780511806575
37. Starke, E. A., and Staley, J. T., "Application of Modern Aluminum Alloys to Aircraft," Progress in Aerospace Sciences, Vol. 32, No. 2-3, 1996, pp. 131-172. doi:10.1016/0376-0421(95)00004-6.
38. ASM Handbook, Volume 19: Fatigue and Fracture, ASM International, Materials Park, OH, 1996.